Seasonal dynamics of organic carbon and metals in thermokarst lakes from discontinuous permafrost zone of western Siberia

R.M. Manasypov[1], S.N.Vorobyev[1], S.V. Loiko[1], I.V. Kritzkov[1], L.S. Shirokova[2,3], V.P. Shevchenko[4], S.N. Kirpotin[1], S.P. Kulizhsky[1], L.G. Kolesnichenko[1], V.A. Zemtzov[1], V.V. Sinkinov[1], O.S. Pokrovsky[1,2]*

[1] Tomsk State University, 634050, Tomsk, 36 Lenin av., Russia

[2] Geosciences and Environnement Toulouse, UMR 5563 CNRS, Université de Toulouse, 14 avenue Edouard Belin, 31400, France, oleg@get.obs-mip.fr

[3] Institute of Ecological Problems of the North UroRAS, 163061, Arkhangelsk, Nab. Severnoj Dviny, 23, Russia

[4] P.P. Shirshov Institute of Oceanology of the Russian Academy of Sciences, 36 Nakhimovsky Prospekt, 117997 Moscow , Russia

Key words: boreal, subarctic, palsa, ice, freezing, winter, spring, trace element

Abstract

Despite relatively good knowledge of the biogeochemistry of Siberian thermokarst lakes during summer base flow, their seasonal dynamics remains almost unexplored. This work describes chemical composition of ~130 thermokarst lakes ranging in size from few m² to several km², located in the discontinuous permafrost zone. Lakes were sampled during spring flood, just after the ice break (early June), the end of summer (August), the beginning of ice formation (October) and during full freezing season in winter (February). The lakes larger than 1000 m² did not exhibit any statistically significant control of the lake size on Dissolved Organic Carbon (DOC), the major and trace element concentrations over three major open water seasons. On the annual scale, the majority of dissolved elements including organic carbon increased their concentration from 30 to 500% with statistically significant ($p < 0.05$)

trend from spring to winter. The concentration of most trace elements (TE) increased in the order spring > summer > autumn > winter. The ice formation in October included several stages: first, surface layer freezing followed by crack (fissure) formation with unfrozen water from the deeper layers spreading over the ice surface. This water was subsequently frozen and formed layered ice rich in organic matter. As a result, the DOC and metal (Mn, Fe, Ni, Cu, Zn, As, Ba and Pb) concentrations were the highest near the surface of the ice column (0 to 20 cm) and decreased by a factor of 2 towards the bottom. The main implications of discovered freeze-driven solute concentrations in thermokarst lake waters are enhanced colloidal coagulation and removal of dissolved organic matter and associated insoluble metals from the water column to the sediments. The measured distribution coefficient of TE between amorphous organo-ferric coagulates and lake water (< 0.45 μm) were similar to those reported earlier for Fe-rich colloids and low molecular weight (< 1 kDa, or < 1-2 nm) fraction of thermokarst lake waters, suggesting massive co-precipitation of TE with amorphous Fe oxyhydroxide stabilized by organic matter. Although the concentration of most elements was lowest in spring, this period of maximal water coverage of land created significant reservoir of DOC and soluble metals in the water column that can be easily mobilized to the hydrological network. The highest DOC concentration observed in smallest (< 100 m^2) water bodies in spring suggests their strongly heterotrophic status and therefore, potentially elevated CO_2 flux from the lake surface to the atmosphere.

1. Introduction

Western and central Siberia's thermokarst (thaw) lakes extend over a territory spanning over a million km^2 (half of the western Siberia Lowland, 0.5 million km^2 and all northern Siberia Lowland, 0.84 million km^2). They are highly dynamic hydrochemical systems that receive chemical elements from the atmosphere and surrounding peat soil and exchange greenhouse gases (GHG) with the atmosphere, delivering dissolved carbon and

55 metals to adjacent hydrological systems. Because more permafrost will continue to thaw due
56 to climate warming, which is heavily intensified in this region (Frey and Smith, 2005), the
57 directions and magnitude of lakes – rivers exchange processes may be significantly modified,
58 seriously affecting the biogeochemical fluxes both on land and in the coastal zone of the
59 Arctic Ocean.

60 In contrast to the relatively good understanding of western Siberia thermokarst lakes
61 functioning during active (summer) season (Walter et al., 2006, 2008; Walter Anthony et al.,
62 2012; Audry et al., 2011; Pokrovsky et al., 2011, 2013, 2014; Shirokova et al., 2009, 2013;
63 Karlsson et al., 2012, 2014; Manasypov et al., 2014), the intra-annual variations of lake water
64 chemistry including glacial period and spring flood remained, up to present time, virtually
65 unexplored. At the same time, glacial season is extremely important in GHG regulation in
66 boreal and subarctic lakes, due to significant accumulation of gases under the ice and their
67 liberation during the ice melting (Karlsson et al., 2013). Similarly, the ice formation period
68 provides important insights into the solute concentration and colloid coagulation
69 mechanisms, given the main particularity of shallow (0.3 to 1.0 m deep) thermokarst lakes in
70 western Siberia – their full freezing during winter (Pokrovsky et al., 2011, 2014). The
71 possibility of complete freezing of western Siberia thermokarst lakes contrasts the majority
72 of other circumpolar water bodies, such as from the Kolyma low land (Walter Anthony et al.,
73 2014), the Lena Delta (Boike et al., 2013) and Mackenzie Delta plain (Tank et al., 2009,
74 2011; Grosse et al., 2013; Walter Anthony and Anthony, 2013) which often have a depth of
75 more than 2 meters and as such do not freeze to the bottom, while exhibiting chemical and
76 thermal stratification of the water column. Another important difference of thermokarst
77 western Siberia lakes from well studied river delta / river valley lakes is the lack of
78 connection to the underground network in the formers. Therefore, lake connection to the
79 hydrological network may occur only via surface flow (Kirpotin et al., 2008), without
80 subsurface flow. Among all studied circumpolar water bodies, shallow ponds of the north of

Canada (Laurion et al., 2010; Negandhi et al., 2013; Bouchard et al., 2014) seem to be most similar to western Siberian thermokarst lakes. However, in a recent compilation of studied circumpolar ponds (Rautio et al., 2011), only one region among 16 (thaw ponds of Boniface, Quebec) exhibits a pH of 5.4±0.6, Cond. of 18 µS cm^{-1} and a DOC of 13.4±4.7 which is comparable to highly diluted ($5 < Cond < 20$ µS cm^{-1}), acidic $3.5 \leq pH \leq 5.5$, and humic and ($10 \leq DOC \leq 40$ mg/L) western Siberia water bodies.

Towards filling the gap in our knowledge of seasonal variations of thermokarst lake chemical composition, we present in this work results of analysis of water and ice sampled in thermokarst lakes of various size, from several meteres to several km in diameter, during four main hydrological seasons: June, August, October and February. Our primary goal was to better understand the thermokarst lake biogeochemical functioning which should allow to constrain the impact of lake water metal and carbon cycling on river water composition and greenhouse gas exchange with the atmosphere in the course of year. On a larger perspective, we aimed at the understanding seasonal pattern of dissolved organic carbon and metal micronutrient concentration in these shallow but highly abundant water bodies, different from previously studied glacial and deep thermokarst/yedoma lakes. This knowledge should allow predictions of phytoplankton activity, sedimentation and microbial respiration on the annual scale, necessary for evaluation of the net ecosystem exchange under various climate change scenarios. To this end, we adressed the following specific questions: (i) is there a statistically significant difference in major and trace element concentration between different seasons, within a broad range of lake sizes? (ii) how significant is lake size and lake water residence time control for lake water chemical composition during different seasons? (iii) what are the mechanisms and degrees of element differentiation during ice formation and full water column freezing? (iv) how significant is water dilution during spring melt and what are the consequences for river water feeding by lakes during this period?

2. Study site description, sampling, analytical and statistical methods.

Our study site is located in the central part of Western Siberia (63.5°N, 75.4°E, Nojabrsk administrative region) withing the northern taiga geographical sub-zone (**Fig. 1**). It contains discontinous permafrost over Late Pleistocene sand and clay deposits that are covered by a layer of peat that is 1–2 m thick. All the lakes in this study are located at watershed divides between adjacent rivers. The water bodies ranged from a few m to several km in diameter and had a similar depth of 1.0 ± 0.5 m under normal precipitation/evaporation conditions (450 mm). During dry summer, the lakes can decrease their depth twofold (Pokrovsky et al., 2013). The morphology, hydrology and the water balance of thermokarst lakes have been extensively studied during four field campaigns in June, August, and October 2013 and February 2014. The detailed depth mapping of ~20 large lakes was performed via GPS-echosounder from a rubber boat; the denivelation and the direction of the water flow were measured using levelling network in several narrow profiles; the depth and density of snow were measured over a model site 500 m x 500 m that included lakes, palsa bog, some streams and adjacent forested riparian zone. The water residence time was calculated from the annual precipitation and evapotranspiration measured at the neighboring meteostation of the Russian Hydrometeorological Station, the annual runoff of the territory (between 200 and 250 mm, Novikov, 2009 and Frey et al., 2007) and the water volume of the lakes measured on-site using a GPS-echosounder.

Water samples were collected from the PVC boat for large lakes or directly from the lake center for small (< 50 m diameter) water bodies (thaw ponds) during June and August 2013 and from the ice during October 2013 and February 2014 sampling campaigns. A list of sampled water bodies and their main hydrological and hydrochemical characteristics is presented in Table 1. The sampling and filtration methods used in this study, as well as the chemical analysis techniques, are identical to those utilized in our previous studies (Pokrovsky et al., 2011). An ultraclean sampling procedure was used for all manipulations in the field (Shirokova et al.,

2010). Water samples were filtered on-site through sterile single-use Minisart® filter units (Sartorius, acetate cellulose filters) with a pore size of 0.45 µm. For TE analysis, samples were acidified to pH = 2 with double distilled HNO_3. Dissolved oxygen, pH, and Eh were measured on-site with uncertainties of 5%, 0.02 units, and 2 mV, respectively, using a WTW® oximeter and a Hanna® portable pH meter with an Eh/pH electrode.

Major anion concentrations (Cl^- and SO_4^{2-}) were measured by ion chromatography (HPLC, Dionex ICS 2000) with an uncertainty of 2%. DOC was analyzed using a Carbon Total Analyzer (Shimadzu TOC 6000) with an uncertainty lower than 3%. Major and trace elements were determined with an ICP-MS Agilent ce 7500, routinely used in our laboratory for the analysis of samples from boreal organic-rich lakes (cf. Pokrovsky et al., 2013). Indium and rhenium were used as external standards. The international geostandard SLRS-5 (Riverine Water Reference Material for Trace Metals certified by the National Research Council of Canada) was used to check the accuracy and reproducibility of each analysis (Yeghicheyan et al., 2014). We obtained good agreement between replicate measurements of SLRS and certified values (relative difference < 10% SD for repeated measurements), except for B and P (30%). While P was discarded for further analyses, B concentrations in most lakes are a factor of 3 to 7 higher than those in the SLSRS-5 and thus were retained. In addition to TE analysis using the Agilent quadropole instrument, 60% of samples were processed with an ultrasensitive Element XR ICP-MS instrument operated in a low and medium resolution mode. Using this ICP-MS greatly increased the detection limits of a number of elements and improved the precision of the analyses while avoiding interferences. The uncertainty of the Element XR analysis was ≤ 5%, while its detection limit was a factor of 100 lower than the traditional (Agilent) instrument. The average agreement between the two ICP-MS instruments for the majority of the TE was 10-15%.

The lake ice was sampled in February 2014 from the central part of the lakes using titanium circular ice coring. The ice core was cut using Ti saw in 10-cm slices, melted at room temperature and immediately filtered through 0.45-µm filters. Before and after fieldwork, blank

158 samples were run by filling the pre-cleaned PVC container with MilliQ water and submerged Ti
159 blades, at neutral pH and letting it to react for several hours. No detectable contamination of Ti,
160 any major and trace elements was observed. The ice filtrate was processed in the same way as
161 the lake water. In three lakes (out of ~ten studied in February), the bottom layer of unfrozen
162 water below the ice column was collected for analysis. Chemical composition of Fe-rich
163 coagulates collected from the ice surface in early June was measured by ICP-MS after full
164 dissolution of the solid using a microwave acid digestion procedure (Stepanova et al., 2014).
165 Particulate organic carbon was quantified using TOC_{CHS} instrument. The freeze-dried
166 precipitates were characterized by scanning electron microscopy (SEM) using a Jeol JSM840a,
167 and by X-ray diffraction using an INEL CPS 120 CoKα.
168 The element concentrations were analysed using best fit functions based on the least
169 squares method, Pearson correlation and one-way ANOVA (SigmaPlot version 11.0/Systat
170 Software, Inc). Regressions and power functions were used to examine the relationships between
171 the elemental concentrations and the lake surface areas. The ANOVA was carried out using
172 Dunn's method because each sampling period contained different number of water bodies.
173 Principal component ananlysis (PCA) was used for the ensemble of sampled lakes and for each
174 season individually, to reduce the number of variables and to detect the structure in the
175 relationships between the elements. The data consisted of ~130 lake water samples grouped into
176 three distinct seasons (spring, summer and autumn). Statistical PCA analyses were applied in
177 order to derive a distinctive view of the influence of various parameters, notably the seasons, on
178 the lake water chemical composition variability. Both normed and non-normed PCA treatment
179 was attempted. Statistical analysis considered each chemical element as a variable (35 in total)
180 for all lakes. For this step, the STATISTICA package (http://www.statsoft.com) which is also
181 designed to compute and render graphics, was used to interpret the spatial structures.
182
183

3. Results

3.1. Effect of the lake size on dissolved carbon and related elements concentration in the water column.

The list of sampled water bodies with their main hydrophysical and hydrochemical characteristics and their geographical localization are given in **Table 1 and Fig. 1**, respectively. Within the range of 100 to 2×10^6 m² lake size, the effect of lake size on major and trace element concentration is not strongly pronounced. The correlation coefficient was below 0.5 for all elements over all seasons, suggesting a quite weak if not negligible impact of the lake size on lake water chemical composition (**Table S1 of the suppelment)**.

Highly variable number of sampled lakes during each season was basically due to the difficulties in sampling logistics and the access to the site. Only five lakes (labelled A, B, C, D, E in Table 1) could be collected during all three open water seasons. In winter, we could not sample more than 3 lakes (both ice core and bottom water). All small lakes (< 1000 m²) were frozen solid in October (autumn period). We did not focus in this work on small size (< 500 m²) lakes in summer, because the small water objects were thoroughly studied in our previous work (Shirokova et al., 2013). Besides, many small ponds (10-100 m²) were dried in August 2013. For this reason, the size range of the sampled lakes is different among seasons.

Only in spring, for the range of 0.1 to 2×10^6 m² lake size, was Pearson's coefficient statistically significant ($p < 0.05$) and suggested a decrease of the following element concentration with the logarithm of the lake size increase: DOC (-0.69), V (-0.43), Cr (-0.54), Ni (-0.58), Cu (-0.63), Ga (-0.71), As (-0.53), Cd (-0.69), Pb (-0.8)**.** Such a semi-logarithmic negative relationship suggests a rapid decrease in the concentration within the small water bodies and its relative stability in large lakes. Indeed, this trend was mainly due to the increase of certain element concentrations in the smallest (< 10-100 m²) water bodies rather than a steady evolution of concentrations in medium-size and large water bodies.

The DOC concentration exhibited two maxima, at 1000-10,000 m² surface area in summer and autumn and in micro-depressions (< 1 m²) in spring (**Fig. 2**). The nature of the DOC was different among different seasons, because the slope of the UV_{280} - [DOC] dependence increased in the order: spring (0.024) < summer (0.030) < autumn (0.035) < winter (0.0354). The ratio of UV_{280} to [DOC] during 4 sampled seasons demonstrated the lowest values in spring and the highest in Fall-winter, being independent of the lake size (**Fig. 3**).

None of the season demonstrated a statistically significant dependence between the element concentration and the water body size above 100 m² ($p > 0.05$). There was quite high variability in the major element concentration in lakes of the same size range, typically over 2 orders of magnitude, as can be seen for Ca and Si in **Fig. S2 a and b (Supplement),** respectively. There was a general increase in the lake water pH with the increase in the lake size (statistically significant at $p < 0.05$), most visible during summer (**Fig. 4**). The small-size lakes sampled in spring exhibited the lowest pH, between 3.5 and 4.5 whereas the larger lakes (> 1000 m²) in summer demonstrated a pH of 5 to 6. Similar to major cations, the major anion concentration did not demonstrate any discernable trend ($p > 0.05$) with the lake surface area; only Cl^- yielded the minimal concentration for the lakes of c.a. 100 m² surface area. Dissolved inorganic carbon (DIC) concentration was a factor of 30 lower than [DOC], without statistically significant trend with the lake size (not shown). The illustration of the lake surface area effect on trace element concentration during all four sampled seasons is given in **Fig. S3** in the Supplement for Fe, Al, Mn, Zn, Cu, Pb, Mo, V, As, and Sb and the primary data are listed in **Table S2**.

There was limited degree of element correlation with either DOC or Fe considering all seasons of the year, as follows from Pearson pair correlation (**Table S3**). Examples of mostly pronounced correlations between Fe and DOC, As and Fe, and Cd and DOC are illustrated in **Fig. S4.** Considering all seasons simultaneously, several groups of elements could be distinguished based on this correlation analysis:

235 *(i)* elements correlated with Fe ($R_{Fe} > R_{DOC}$): Cl, SO_4, Mg, Ca, Sr, Ba, Rb, Al, Ga, Cr,
236 Mn, Co, Ni, Si, As, REEs and U
237 *(ii)* elements correlated with DOC rather than with Fe ($R_{DOC} > R_{Fe}$): Cu, Zn, Cd and Pb
238 *(iii)* elements strongly correlated to Al ($R > 0.6$ at $p < 0.05$): Be, Si, K, Rb, Cs, Sr, Ba, Ti,
239 V, Cr, Co, Cu, Ga, As, Sb, REEs, W and U
240 *(iv)* elements exhibiting high pair correlations ($R \geq 0.9$ at $p < 0.05$): Ga-Al, Cr-Al, Hf-Th
241 Note that all elements exhibited better inter-correlations in spring compared to other seasons
242 (**Table S3**).
243
244 *3.2. Lake freezing during the glacial period (October to the end of May) and ice-layered*
245 *structure formation*
246 Observations during the beginning of the ice formation (October 2013) yielded important
247 and novel features of thermokarst lake ice cover evolution during glacial period. Given the
248 closed basins of all sampled lakes underlain by permafrost without connection to the
249 groundwater source (i.e.., Pokrovsky et al., 2011, 2014), the water was expected to be under
250 excess pressure under the ice. This was confirmed by direct observations in October: the water
251 always rose upward and spread over the ice surface after drilling the first 10-20 cm of the ice
252 layer. Upon the thickening of the ice, cracks formed on the ice cover and the water from the
253 deeper layers seeped and spread over the ice surface, thus forming organic- and Fe-rich
254 multilayered ice up to 30 cm thick. The wind acting on still unfrozen freshly ejected water
255 created ice ripples spreading over a surface of 10-50 m^2 (**Fig. S5**). The full freezing of ejected
256 organic-rich water led to browning of the ice and presumably produced significant coagulation of
257 colloids. The products of this coagulation could be notably seen at the end of the spring, during
258 massive ice melt (**Fig. S6**).
259 In-situ oxygen analysis with submersible O_2 sensor in June and August demonstrate
260 saturation with atmospheric oxygen close to 90 ± 10% (**Table 1**). In October, under the ice, we

found only 40-80% saturation of the water layer, with some redox stratification within 20-50 cm of the unfrozen water column. There was a 50% drop in O_2 concentration at the sediment-water interface relative to the bottom of the ice core. Generally, the smaller the water body, the lower the oxygen concentration, although a straightforward relation between the size of the lake and the oxygen saturation in October could not be established ($p > 0.05$).

The ice core analysis with the resolution of 5-10 cm demonstrated either an enrichment of the surface ice layers in dissolved elements, or their non-systematic variation over the full depth of the ice core (**Table S4**). The enrichment, by a factor of 2 to 5, of the first 0-30±10 cm was detected for DOC and most metals such as Al, Fe, Ni, Co, Cu, Zn, Pb as illustrated for selected metals in **Fig. 5**. Manganese demonstrated the largest variation along the ice core depth. Its concentration decreased from 3 to 10 ppb at the very surface down to less than 0.1 ppb below 50 cm. In contrast, many trace elements (Cd, Cs, Sb, Ti, Zr, Hf, Th, U, REEs) did not demonstrate statistically significant ($p < 0.05$) trend of concentration with depth for three sampled ice cores. Ca^{2+}, SO_4^{2-}, DIC, Cl^-, and Na^+ also demonstrated nonsystematic variation with depth. In winter, only three (out of ~ ten) sampled lakes yielded the liquid water presence above the sediment. The thickness of the unfrozen layer ranged from 10 to 20 cm, with an ice thickness of 60 to 80 cm.

Using the element concentration measured in remaining water at the sediment – ice interface and the bottom 10 cm layer of the ice core, element distribution coefficients between the ice and the remaining fluid can be assessed. Note that the obtained values can be considered as preliminary estimations, given very limited number of samples. The agreement in K_d (water/ice) between three sampled lakes for which both fluid and bottom ice were available is reasonably good for a number of major elements, as it can be seen from the average with 2 SD (n = 3) listed in **Table 2.** The lowest K_d (water/ice) is observed for DIC (1.64±0.37) and Cl (7.6±3.0). The DOC distribution varied significantly among the lakes (K_d (water/ice) is between 5 and 21). Al, Ti, Mn, Ce and some REE yielded K_d (water/ice) between 50 and 100. The

majority of other trace elements exhibit the K_d (water/ice) between 10 and 40 without any discernable link to element chemical properties and degree of binding to DOM.

The most significant transformation of the lake water chemical composition presumably occur during the full freezing of the water column over the winter period. At the end of the winter, during massive snowmelt, products of colloidal coagulation are largely present at the surface of the ice blocks within the lake borders (**Fig. S6**). The coagulates collected in large (~10^6 m²) thermokarst lakes in early June are essentially composed of iron oxohydroxide and organic matter with significant amount of co-precipitated trace elements. The aggregates are XRD-amorphous and contain 17.5±0.5% of POC.

Based on total chemical analysis of solid coprecipitates, we calculated the distribution coefficients of trace element (TE) between the Fe-rich coagulates and the lake water, normalized to Fe (as the major component of the coagulates):

$$K_d = [TE]/[Fe]_{coagulate} / [TE]/[Fe]_{lake\ water}$$

where $[TE]/[Fe]_{lake\ water}$ represents the ratio of average TE and Fe concentrations in large lakes at the end of summer, before the beginning of ice formation. The K_d values of major and trace elements range from 0.05 to 0.5 (**Fig. 6**). The values of distribution coefficient obtained in the present study are in reasonable agreement with those reported for colloids (1 kDa – 0.45 µm) and LMW (< 1 kDa) fraction of another large thermokarst lake located in discontinuous permafrost zone (Pokrovsky et al., 2011) as well as the rivers and streams of the boreal non-permafrost zone (Vasyukova et al., 2010). For the majority of dissolved elements, the K_d of particles are within a factor of 2 different from previously reported K_d of colloids.

311 *3.3. Seasonal trend in element concentration in the thermokarst lake water: progressive increase*
312 *from June to February*

313 The first statistical test was aimed to assess the difference in element concentration between
314 different seasons for the full range of the lake size. It was found, using H-criterion of Kruskal–
315 Wallis and Mann-Whitney U Test, which allowed one to estimate the difference between two
316 independent set of data based on one given parameter, that all elements are different between
317 three main seasons at the significance level of $p < 0.05$. This allowed one to calculate the average
318 element concentration with $\pm 2\sigma$ standard deviation or all studied lake sizes from 100 to >
319 500,000 m² for spring, summer and autumn, as listed in **Table 3**. Note that the winter data are of
320 low representativity, given that only three unfrozen lakes could be used for this calculation. The
321 median was similar to the average within the 2σ standard deviation of the average.

322 The majority of dissolved elements exhibited a statistically significant increase of their
323 average concentration from spring to autumn (20 to 50%). These are DOC, Mg, K, Ca, Al, Ti, V,
324 Cr, Mn, Fe, Ni, Co, Cu, Ga, Rb, Sr, As, Cd, Sb, Mo, Cs, Ba, all REEs, Pb, and U. Examples of
325 the average element concentration evolution grouped by several families of elements with similar
326 chemical properties and affinity to DOC and Fe colloids (i.e., Pokrovsky et al., 2013) are shown
327 in **Fig. 7.** The trends of element concentration in the lake water from spring to autumn are quite
328 similar for large (> 500,000 m²) and medium (100-500,000 m²) water bodies. We estimated the
329 minimal impact of lake water freezing assuming a conservative scenario of element
330 concentration evolution in thermokarst lakes. Based on thorough hydrological observations, we
331 accepted, for 1 m² of the average lake depth of 75±25 cm in summer, to which we added 20 cm
332 flooding in spring and from which we subtracted 20 cm of the water layer for ice formation in
333 October. The 3 sampled lakes exhibited almost full freezing in February with c.a. 10 cm of
334 bottom water left and 65 cm of the ice. The concentration factor was calculated as the ratio of the
335 water volume under 1 m² in a given season to that in spring. It was equalled to 1, 1.3, 2.0 and 9.5
336 for June, August, October and February, respectively.

Conservative behavior of selected major and trace elements is illustrated in **Fig. 7** as a dashed line. Most major elements (Si, K) and a number of trace metals (Al, Ti, Cr, Cu) exhibited close to conservative behavior. In contrast, DOC demonstrated significant depletion during winter, between October and February. Fe, Ni, Cd and Pb were slightly non-conservative showing a depletion in winter. The effect of the season can be quantified as the ratio of the average summer and autumn to spring concentration ($R_{summer/spring}$). This ratio is the highest for Ba (6.7) and light REEs (7 to 3), followed by Zn (4.3), Si (4.3), Al, Fe and trivalent hydrolysates (4.2 to 2.8), tetravalent hydralysates, Cr and divalent heavy metals such as Co, Cu, Ni, Cd, Mn (2.5 to 3.3). A number of elements did not demonstrate a significant increase in the concentration during the baseflow season compared to the spring period, exhibiting $R_{summer/spring}$ values below 2 (B, Mg, Na, Ca, Cs, Pb, V, As, Sb, Th and Zr).

Despite significant uncertainty in the average summer-period element concentration in thermokarst lakes (see **Table 3**), the values obtained in the present study are consistent with thermokarst lake water chemical composition across the gradient of the permafrost zone, from discontinuous/sporadic to continuous permafrost. The values of DOC, all major and trace element concentration agree, within the uncertainty of the average, with the values of element concentration interpolated from the latitude – lake water concentration dependence (Manasypov et al., 2014) for the latitude of the study site. It follows that relatively small area investigated in this work can be a good surrogate for much larger region of western Siberia (described in Manasypov et al., 2014) in terms of seasonal evolution of thermokarst lake chemical composition.

3.4. Water residence time effect on lake water chemical composition

The effect of lake water residence time (WRT) on the summer-period and average spring-autumn chemical composition of thermokarst lakes exhibits two clusters of the data points (**Fig. 8**). Statistical analysis of observed dependencies confirmed a significant link between the water

residence time and both summer and season-average DOC concentrations with the Spearman correlation coefficient (R_S) equal to -0.65 ($p < 0.05$). The most important result is that, at WRT < 8 months, an almost five-fold increase in DOC concentration occurs. A similar impact is observed for Fe with R_S = -0.55 ($p < 0.05$). This result can be understood given that the Fe is likely to be present in the form of organic colloids. The alkaline and alkaline-earth major cations and other metals, however, did not demonstrate any statistically significant ($p > 0.05$) link to the WRT. The estimation of WRT for the smallest (< 10-100 m²) water bodies was impossible due to the ephemeral nature of these small thaw ponds. However, considering their typical existence between the start of the snow melt (May) and summer drought (July – August), the water resides in these water bodies between 0.1 and 0.3 years. The highest concentration of DOC observed in spring in < 10 m² depressions (**Fig. 2**) is therefore consistent with the trend shown for large lakes in **Fig. 8.**

3.5. PCA analysis of possible TE sources in thermokarsk lakes

The data consisted of ~130 lake water samples grouped into three distinct seasons (spring, summer and autumn). Statistical analysis considered each chemical element as a variable (35 in total) for all lakes. Considering all seasons together, the first factor was responsible for 16% variation and included B, Na, Si, K, Ca, Ti, V, Cr, Ni, Zn, Rb, Mo, Sb, Cs, Ba, La, Ce and U whereas the 2nd factor (6.3%) included Al, Fe, Co, As, and Cd (**Fig. S7**). Separation of F1 and F2 factors in June and August was uncertain since they provided only 9% and 6.7% (June) and 11.8% and 5.8% (August) variations. In contrast, October's data could be explained by 18.8% variation of F1 (B, Na, Si, K, Ca, Ti, V, Cr, Ni, Zn, Rb, Sr, Zr, Mo, Sb, Cs, Ba, La, Ce and U) and 4.4% F2 (SO4, Cu, Co, Fe, As). The list of elements and corresponding factors for each season are given in **Table S5.**

This PCA treatment demonstrated rather high variability of lake chemical composition, mostly pronounced during June and August. In June, multiple factors are responsible for element

389 enrichment in the lake water, namely the lateral input from thaw snow and lake ice, dissolution
390 of colloid coagulation products, and leaching of plant litter. The F1 factor in June is very poorly
391 pronounced. Nevertheless, it may mark the colloidal transport of TE (organic complexes)
392 whereas the 2nd factor may correspond to the degree of snow input (typical atmospheric aerosol –
393 originated elements). In August, internal (autochthonous) processes and subsurface feeding are
394 likely to strongly modify lake water chemical composition both for major (pH and DIC of the F2
395 factor) and TE. In addition, atmospheric precipitation in the form of rain which dilute lithogenic
396 TE but also deliver marine aerosols and dust (subjected to dissolution) can strongly modify the
397 role of individual correlations. Finally, October represents the period when the first factor is
398 mostly pronounced, as also translated in the PCA results of all seasons together. Presumably, the
399 period of the beginning of ice formation corresponds to the maximal stability of the F1 x F2
400 structure; during this time, the influence of both allochthonous (lateral and subsurface TE influx
401 from peat, mineral soil horizons and ground vegetation) and autochthonous (bio- and
402 photodestruction of organic colloids, primary productivity) processes are minimal.
403
404 *3.6. Element speciation in thermokarst lake waters*
405 We used the geochemical program Visual MINTEQ (Gustafsson, 1999), version 3.1
406 (October 2014)) for Windows, (see Unsworth et al. (2006) for vMINTEQ application example)
407 in conjunction with a database and the NICA-Donnan humic ion binding model (Benedetti et al.,
408 1995; Milne et al., 2003) and Stockholm Humic Model (SHM). Speciation calculations were
409 performed for Ba, Ca, Cd, Co, Cu, K, Mg, Mn, Na, Ni, Pb, Sr, Zn, and Al, Fe^{III}, Th^{IV}, and $U^{VI}O_2$
410 for average lake water composition in spring, summer, autumn and winter as well as the average
411 August composition of large (> 500,000 m²) and small (100-500,000 m²) lakes (Table 3). In
412 addition to NICA-Donna approach, Stockholm Humic Model (SHM) of visual MINTEQ was
413 used to calculate metal speciation in the lake water.

Results of the calculation of metals degree of complexation with DOM are listed in **Table S6** and illustrated in **Figures S8 and S9.** According to NICA-Donnan model, the majority of divalent major and trace element is bound to organic, Donnan-like complexes. Only Na and K exhibits a decrease of 80 to 10% complexed fraction from spring to winter. Extremely high complexation of metals with DOM (up to 80 to 90%) within the Nica-Donnan concept is supported by dialysis experiments conducted in various thaw lakes of western Siberian subarctic (Pokrovsky et al., 2013; Shirokova et al., 2013). In contrast to the Nica-Donnan, the Stockholm Humic Model (SHM) predicts moderate and quite variable association of divalent metals with DOM, with the lowest values for Ba and Mn (40% in spring and 20% in winter) and the highest values for Cu and Pb (80-90% for all seasons). It is important to note that the highest proportion of organic complexes is observed in summer, presumably due to the highest pH recorded during this season which favors the deprotonation of functional groups of the DOM. The lowest proportion of organic complexes in winter could be due to competition between metals for organic ligand binding sites, given significant increase of Me^{2+} compared to DOC during solute concentration by freezing.

The lake size has pronounced impact on some metal complexation with DOM as illustrated in **Figure S9.** Even within the "conservative" SHM model, the TE in small thaw ponds exhibit 100% complexation with DOM. The degree of complexation is smaller in large lakes having a factor of 2 lower DOC concentration, despite that their pH is higher than that of small lakes (5.49 and 4.72, respectively). Interestingly, this may indicate higher bioavailability of metal micronutrients in large lakes, in line with the hydro biological evolution of western Siberia thermokarst lakes, namely the elevated productivity and the presence of macrophytes and phytoplankton blooms in large mature thermokarst lakes (Pokrovsky et al., 2014). Another important conclusion from the speciation modeling is that the DOC concentration has more pronounced impact on metal speciation (notably the % of organic complexes) than the pH - both across the seasons and different lake size groups.

4. DISCUSSION

4.1. Lake water composition control by snow and ice melt in spring.

The lack of a trend in DOC and metal concentration with the lake surface area increase above 100 m² (**Fig. 2, Table S1,** R^2 = 0.17, Rs = -0.33) in spring implies that the lakes are essentially influenced by allochthonous (surface runoff from snowmelt) sources of dissolved material with minimal transformation of DOC and metal complexes by intra-lake autochthonous processes. In the opposite case, one would expect a tendency of DOC and chemical element increase with the decrease of the size of the water body, notably below 100 m², as it is encountered in summer periods in sporadic and discontinuous and permafrost zone of thermokarst lake development (Shirokova et al., 2013). Given that the upper part of the peat column is still frozen in the beginning of June, the source of the solutes to the lake water is most likely to be ground vegetation, comprising dwarf shrubs, mosses and lichens, as well as the litterfall of the previous year. The input of the vegetation leaching products should be similar for the lakes of different sizes, given the very homogeneous palsa bog dominant landscape at the study site.

The spring flood period is known to be the most important in terms of land coverage by water, on the annual scale (Zakharova et al., 2009, 2014). As a result, the average chemical composition of the dominant surface waters in the discontinuous permafrost zone of western Siberia can be approximated by that of the spring period as listed in **Table 3**. Elevated DOC concentration in thermokarst lakes during spring priod, a factor of 2 to 3 higher than the typical 10-15 mg L^{-1} of boreal waters (Dillon and Molot, 1997), suggests high potential of releasing CO_2 to the atmosphere, notably in numerous small depressions filled by thaw water.

A systematic ($p < 0.05$) increase of the average slope of dependence $UV_{280\ nm}$ – [DOC] in the course of the season (**Fig. 3**), from 0.024 in spring to 0.0354 in winter (the latter with only 3 samples) suggests an increase in the input of aromatic compounds (presumably from peat

466 lixiviation) to the end of the vegetative season relative to the leaching of fresh vegetation
467 products (low aromatic, plant and litter exudates) mostly visible after the snowmelt, when the
468 surrounding peat is still frozen. Correcting the UV absorbance for dissolved Fe^{3+} (Weichaars et
469 al., 2003) via subtracting a term of 0.08×[Fe, ppm] will change the $UV_{280\ nm}$ value by less than
470 10% which is beyond the variability of the seasons and lake size. Note also that a recent study of
471 DOC-UV properties in a boreal site demonstrated the absence of the influence of nitrate and iron
472 on UV and visual absorbance up to 2.2 mg/L of Fe(III), Avagyan et al. (2014). The lack of any
473 trend ($p > 0.05$) in UV/DOC ratio as a function of the lake size (**Fig. 3)** strongly suggests the
474 similarity of the DOC sources in the full range of the lake size in each season. As a result, the
475 season rather than the lake size at $S > 100$ m² seems to be the most important factor controlling
476 both the average concentration and the chemical nature of DOC and related elements.
477 Comparison of TE concentration in summer relative to spring (section 3.3) distinguishes
478 two groups of elements: elements which do not significantly increase their concentration in
479 summer relative to the spring and elements whose concentrations are affected by the seasons by
480 a factor of 2 or higher. For example, the increase of Si and metal micronutrients (Zn, Co, Ni, Cu,
481 Cd, Ba and Mn) in summer relative to spring might indicate some preferential release of these
482 elements during active plant and upper moss litter leaching in relatively warm waters. In
483 contrast, high concentrations of B, Na, Mg, Ca, Cs, Pb in early spring compared to the end of the
484 summer may indicate their input with atmospheric deposition after snow melt.
485
486 *4.2. Concentration mechanism during freezing period; enhanced colloidal coagulation*
487 The unusual distribution of organic carbon and related trace elements over the ice core
488 profile, with an accumulation in the upper 20-40 cm of the ice column, stems from a sequence of
489 events during lake freezing, linked to (*i*) shallow depth and possibility of the full freezing of the
490 water column and (*ii*) the lack of any outlet or hydraulic connection to the groundwater of these
491 confined water bodies underlain by the impermeable permafrost layer in the form of the frozen

492 sand/peat. The hypothetical scheme of crystallization process is illustrated in **Figure 9.** The
493 squeezing of remaining water from the bottom towards the surface through the ice cracks starts
494 as early as October. This produces the layered, organic- and Fe-rich secondary (allochthonous)
495 ice which is crystallized at the already frozen lake surface. During winter, the progressive
496 freezing downwards the water column and the decrease in the connectivity between the
497 remaining water and the lake surface bring about the decrease in element concentration in the
498 bottom ice while concentrating of solutes in the remaining fluid at the ice – sediment interface.
499 The progressive lake freezing produces layered ice having contrasted content of major and trace
500 elements among different layers, reflecting the full freezing of water pockets formed via seeping
501 the bottom water at the lake surface. The DOC and many related elements exhibit a general
502 decrease of concentration downward from the ice core surface. The freezing sequence of the
503 thermokarst lakes constrasts with the freezing of non-permafrost (glacial) lakes, which are
504 generally deeper than 1 m and have an inlet/outlet and underground connection. To which degree
505 the scheme of ice formation suggested for shallow thermokarst lakes in discontinuous permafrost
506 zone can be applied to other, sporadic and continuous permafrost regions of western Siberia,
507 remains unknown. However, given shallow depth and closed-basin settings of most thermokarst
508 lakes, the extrapolation of obtained ice chemistry data and partitioning coefficients to other
509 thermokarst lakes of western Siberia should be possible.

510 To our knowledge, the information on TE partitioning between the lake water and the ice
511 for other boreal settings is lacking. The similar range of DOC and many major and trace metal
512 distribution coefficients between the ice and the remaining solution encountered in the present
513 study (Table 2) is remarquable and contrasts with the recent results of DOM incorporation
514 during sea ice formation (Muller et al., 2013). The latter authors argued that DOM is
515 incorporated to sea ice relatively more than inorganic solutes. In the case of low total dissolved
516 solid (TDS), DOM-rich thermokarst lakes of the present study, the majority of solutes may
517 follow the DOC being present as organic colloids (1 kDa – 0.45 µm), as follows from vMINTEQ

518 speciation calculation (section 3.6) and also demonstrated by dialysis experiments (Pokrovsky et
519 al., 2011, 2013).

520 Various physico-chemical processes may be involved in the transformation of solutes and
521 DOM and metal-rich water pockets incorporated in the ice, notably within its most surface
522 layers. Among them, photoreductive dissolution of iron oxy(hydr)oxide trapped in the ice (i.e.,
523 Kim et al., 2010) can occur both in winter and spring, during massive ice melting. The
524 enrichment of both Fe and Mn in the first 20 cm of the ice column relative to the deeper ice
525 layers (**Fig. 5**) can certainly promote enhanced reductive dissolution of both Mn (Kim et al.,
526 2012) and Fe (Kim et al., 2010) under ice thaw during polar day in early June. However, Fe(II)
527 fraction was estimated to be below 10% in June's lake sampling as the $LMW_{< 1\ kDa}$ fraction
528 containing essentially uncomplexed $Fe^{2+}(aq)$ was ≤ 5% of total dissolved Fe (see method of
529 Fe(II) analysis in the lake water by *in-situ* dialysis technique in Pokrovsky et al., 2012).
530 Therefore, oxygenated spring waters and shallow depth of thermokarst lake provide favorable
531 conditions of Fe(III) colloids formation in these organic-rich water bodies. Highly non-
532 conservative behavior of DOC during the winter time demonstrating significant depletion in
533 February **(Fig. 7 A)** may suggest some heterotrophic respiration of DOM under the ice.
534 Alternatively, the DOC could be transformed into POC and precipitated to the lake bottom or be
535 trapped as particles in the growing ice.

536 During the massive ice melting, a significant number of coagulated organo-ferric
537 particles remain on the ice surface (**Fig. S6**) and eventually precipitate to the lake bottom.
538 Although under anaerobic conditions in the thermokarst lake sediments, Fe(III) may be reduced
539 and return to the water column (Audry et al., 2011), the majority of Fe oxyhydroxide is likely to
540 remain in the particulate form, thus preventing Fe to move to the hydrological network during
541 spring floods. We hypothesize that one of the most powerful mechanisms of organic and
542 organo-mineral colloid coagulation in thermokarst water bodies is annual freezing of the whole
543 water column leading to significant concentration of Fe, C_{org} and related divalent metals and

trivalent and tetravalent hydrolysates in the particulate phase. In the northern part of discontunuous permafrost zone, the lake sediments are indeed enriched in Fe and trivalent and and tetravelent hydrolysates (Audry et al., 2011). It is remarquable that Fe-normalized distribution coefficients of TE between the organo-ferric coagulates and filtered (< 0.45 µm) lake water (Fig. 8) are of the same order of magnitude or within a factor of 2 different from the distribution coefficients of TE between Fe-rich colloids (1 kDa – 0.45 µm) and $LMW_{< 1\ kDa}$ fraction assessed in previous studies in thermokarst lakes (Pokrovsky et al., 2013) and boreal surface streams (Vasyukova et al., 2010). This similarity strongly suggests that the elementary mechanisms of TE incorporation in organic matter-stabilized Fe oxyhydroxids include mainly co-precipitation and that it is generally similar for colloids and particles.

4.3. Allochthonous versus autochthonous processes forming lake water chemical composition

Allochthonous processes forming lake water chemical composition include the input of fresh vegetation products and the leaching of the upper peat layer. At the beginning of the active season, in June, there is a lateral input of melting snow, reflecting the interaction of water with ground vegetation such as mosses and lichens as well as with the litter fall of the dwarf shrubs from the previous year. During summer (baseflow) season, there is a peat leaching at the lake border via mainly wave abrasion and element and DOC release from moss and lichen coverage via lateral flow fed by rains.

The DOM entering the lake ecosystem with the snow melt and surface inflow during summer rain is subjected to two processes of autochthonous transformation during open water period: photo- and bio-degradation, mostly pronounced in June – September (i.e., Larouche et al., 2015). During summer, the productivity of phytoplankton including possible exometabolite release represents less than 10% of heterotrophic bacterioplankton respiration in western Siberian thermokarst lakes of the discontinuous/sporadic permafrost zone (Shirokova et al.,

570 2013). The heterotrophic bacterioplankton activity brings about the conversion of colloidal DOM
571 and low molecular weight (LMW) organic ligands to particulate organic matter (POM) in the
572 form of coagulates or the bacterioplankton biomass; in both forms, the POM is likely to
573 precipitate to the lake bottom in the course of the active season. During the glacial period, the
574 processes leading to sedimentation of POC to the lake bottom are cryoconcentration and colloid
575 coagulation (see Sect. 4.2 and Fig. S6). The physico-chemical coagulation of DOC may become
576 especially important during progressive lake freezing in winter. Highly non-conservative
577 behavior of DOC (Fig. 7a) relative to the other major components (Si, K, Na) strongly suggests
578 the preferential removal of DOC from the remaining water under the ice cover. The other
579 elements such as metals Fe, Ni, Cd and Pb (Fig. 7 c, i, k, l, respectively) follow non-conservative
580 behavior of DOM suggesting their massive removal from the water column in the form of
581 organic coagulates. In contrast, Al, Ti, Zn, Cr and Cu (Fig. 7 d, e, g, h, j, respectively) remain
582 conservatively in the bottom water or even accumulated in the water. It is possible that they are
583 less dependent on large-size DOM colloids mostly subjected to coagulation during
584 cryoconcentration. Indeed, these metals could be bound to $LMW_{< 1\ kDa}$ organic complexes and
585 thus remain in unfrozen water in the lake bottom layer. Additional input of Al and Ti from
586 mineral clayer sediments of the lake (i.e., Audry et al., 2011) cannot be excluded.

587 The behavior of DIC is almost conservative during lake freezing, without any excess of
588 DIC over theoretical value in February. As a result, there is no significant accumulation of
589 inorganic carbon in the form of CO_2 or HCO_3^- under the ice cover. This result strongly suggests
590 the dominance of physico-chemical coagulation rather than microbial respiration in DOC
591 removal from the water column in winter. The latter process dominates the open water period,
592 when heterotrophic aerobic bacterioplankton respiration of allochthonous DOM produces
593 gaseous CO_2 that is released to the atmosphere in western Siberia thermokarst lakes which are
594 strongly supersaturated with respect to atmosphere (Shirokova et al., 2009, 2013), similar to the
595 other boreal lakes (Jansson et al., 2008; Rautio et al., 2011). The response of this microbial

process to the DOC input in the lake may be fast, on the matter of days, given that *i*) we observed elevated (> 20 mg/L) DOC concentration in smallest (< 2 m²) ground depressions formed within hours after snowmelt, and *ii*) the leaching of DOM from plant litter is very fast, on the order of hours (Berg, 2000; Fraysse et al., 2010).

A plot of DOC concentration versus water residence time in medium and large lakes (300-1,200,000 m²) revealed two clusters of the data points, with maximal DOC concentration observed in lakes and ponds of short-term water circulation and a stable and rather low DOC concentration (10 ± 5 mg/L) in lakes of slow water turnover (**Fig. 8a**). Since the allochthonous input increases DOC in the water body and autochthonous microbial respiration and physico-chemical coagulation remove DOC from the water column, the former process is certainly dominant for short-living water bodies. The hydrological balance of the smallest water depressions (< 200 m²) could not be quantitatively assessed but it can be suggested that the lowest water residence time in these, partially ephemeral, water bodies is consistent with the highest DOC measured in this study. In the lakes of slow water turnover, the input and removal of DOC are presumably balanced. Note, however, the similarity of the intensity of autochthonous processes in larger lakes (i.e., ≥ 100,000 m²), regardless of their size and the water residence time.

4.4. Seasonal evolution of stock of carbon and TE in thermokarst lakes

The average of the six smallest (< 1 m²) depressions sampled in spring shows a factor of 2.3 ($p < 0.05$) higher concentration of dissolved organic carbon (30.8 ± 7.3 mg/L) compared to the larger water bodies (13.2±6.6 mg/L) during this period. This strongly suggests the importance of short-term plant debris (litter) and submerged ground vegetation leaching occurring right after the snowmelt. On the western Siberia lowland, the water stock is the highest during the spring period, notably in terms of water coverage of the land depressions (60 to 70% of the overall watershed area, Zakharova et al., 2014). According to satellite observations in

western Siberia, the area subjected to the spring flood period is 55-65% higher than that of the summer period (Zakharova et al., 2014). Taking into account these observations, and the DOC concentration in thermokarst water bodies, we estimate that the overall increase of soluble stock of DOC and related metals in surface waters in June relative to August may be as high as 200 - 500%. This value stems from (*i*) a factor of 2 - 3 increase in the wetland flooding in June compared to summer baseflow season multiplied by (*ii*) a factor of 1.5 - 2 higher DOC and metal concentration in small (< 1-10 m²) water bodies compared to the larger lakes. This dissolved fraction may be easily mobilized from the watershed to the river and further transported to the ocean.

In shallow thermokarst lakes, progressive ice melt from the surface towards the bottom slowly liberates inorganic carbon trapped or dissolved in the ice. The K_d(water/ice) for DIC (1.2-2.2) is much lower compared to other elements including DOC. As such, the ice is not particularly enriched in DIC relative to the bottom water and both winter and spring period DIC and CO_2 concentrations are not significantly higher than those in summer. Therefore we do not expect significant buildup of CO_2 under ice and CO_2 release from the lake water to the atmosphere during spring melt, contrasting to well known phenomena on deep boreal lakes (Karlsson et al., 2013). The reasons for this contrast could be low volume of the thermokarst lake water and relatively short period suitable for this accumulation in western Siberia, since already in February, there is a lack of liquid water under the ice, yielding a very low fraction (between 10 and 20%) of this unfrozen water stock. Altogether these arguments suggest that the only mechanism capable of enriching the lake water in CO_2 during spring melt is heterotrophic respiration of "fresh" allochthonous DOM, as confirmed by elevated DOC concentration during this period, notably in small water bodies.

Conclusions

A hydrochemical study of shallow thermokarst lakes from a discontinuous permafrost zone of western Siberia revealed conceptually new features of element concentration evolution over different seasons within a large scale of the lake size. Statistical treatment demonstrated that there is no significant difference in element concentration as a function of the lake size within the range of $2 \cdot 10^2 – 2 \cdot 10^6$ m² in June, August and October. However, in spring, there was a clear increase of DOC and related metal concentration with the decrease in the size of small water bodies (< 200 m²). Such small ponds disappear in summer due to evaporation and quickly freeze solid at the very beginning of the glacial season. Most of the dissolved elements and organic carbon decreased their concentration following the order June < August < October, regardless of the lake size range, from $2 \cdot 10^2$ to $2 \cdot 10^6$ m². Therefore, although there are statistically significant differences in organic carbon, major and trace element concentration between different seasons, the lake size has a negligible influence on the lake water chemical composition, except in very small water bodies sampled only in spring. The water residence time (WRT) may be important parameter controlling lake DOC and Fe concentrations, especially for short – lived water bodies, mostly present during spring. In contrast, the other major and trace elements did not demonstrate any clear link with WRT in the lake.

The ice formation in October created an excessive pressure within the confined water body; the remaining organic- and Fe-rich water was seeping onto the ice surface via cracks of the ice cover. This seeping produced the ice of multiple layers with significant enrichment in Fe, DOC and trace elements in the frozen water pockets within the first 0-20 cm in depth. Massive coagulation of organo-ferric colloids occurred during full freezing of the lake water and produced macroscopic, organic- and Fe-rich amorphous particles capable to precipitate to the lake bottom. The main mechanisms of element differentiation during ice formation are concentration and coagulation of organic and organo-mineral colloids, as shown by highly non-conservative behavior of DOC and related metals. The partitioning coefficients of TE between

675 the lake water (< 0.45 µm) and the particulate coagulates reflecting the degree of element
676 differentiation during ice formation and full water column freezing were similar to those
677 measured for Fe-rich colloids (1 kDa – 0.45 µm) in other thermokarst and boreal lakes and
678 rivers.

679 The spring flood period created the highest stock of dissolved allochthonous DOC and
680 related metals, notably in small (< 200 m²) water bodies and depressions. The water dilution
681 during this period (e.g., typically 20% of the water volume increase) can compete with the
682 increase in the land surface coverage for the overal element stock in lakes in June relative to
683 August. We estimate that the overall increase of soluble stock of DOC and related metals in
684 surface waters and consequently, potential for river water feeding by lakes during spring floods,
685 ranged between a factor of 2 to 5. Further assessment of this increase requires high-resolution (<
686 0.5-1 m²) remote sensing observation coupled with *in-situ* hydrochemical measurements. Given
687 significant coverage of the land surface by thaw water in spring and elevated DOC
688 concentrations during this period, the overall impact of snowmelt on CO_2 emission into the
689 atmosphere may be significantly higher compared to that in summer. In contrast, winter time
690 period leading to full freezing of the water column is unlikely to build up significant GHG
691 concentration under the ice and appreciably affect gas regime of thermokarst lakes at the annual
692 scale.

693

694 **Acknowledgements**

695 This work was supported by BIO-GEO-CLIM grant No 14.B25.31.0001 of Russian Ministry of
696 Science and Education, ANR CESA "Arctic Metals", RFBR 14-05-31457 mol_a and grant MK-
697 3684.2015.5. We thank two anonymous reviewers for their constructive comments.

698

699

700

REFERENCES

Audry, S., Pokrovsky, O. S., Shirokova, L. S., Kirpotin, S. N., and Dupré B.: Organic matter mineralization and trace element post-depositional redistribution in Western Siberia thermokarst lake sediments, Biogeosciences, 8, 3341–3358, 2011.

Avagyan, A., Runkle, B.R.K., Kutzbach, L.: Application of high-resolution spectral absorbance measurements to determine dissolved organic carbon concentration in remote areas, J. Hydrology 517, 435–446, 2014.

Benedetti, M.F., Milne, C., Kinniburgh, D., van Riemsdijk, W., Koopal, L.: Metal ion binding to humic substances: Application of the non ideal competitive adsorption model, Environ. Sci. Technol. 29, 446-457, 1995.

Berg, B.: Litter decomposition and organic matter turnover in northern forest soils, Forest Ecol. Manag. 133, 13-22, 2000.

Boike, J., Kattenstroth, B., Abramova, K., Bornemann, N., Chetverova, A., Fedorova, I., Fröb, K., Grigoriev, M., Grüber, M., Kutzbach, L., Langer, M., Minke, M., Muster, S., Piel, K., Pfeiffer, E.-M., Stoof, G., Westermann, S., Wischnewski, K., Wille, C., and Hubberten, H.-W.: Baseline characteristics of climate, permafrost and land cover from a new permafrost observatory in the Lena River Delta, Siberia (1998–2011), Biogeosciences, 10, 2105-2128, 2013.

Bouchard, F., Francus, P., Pienitz, R., Laurion, I., Feyte, S. : Subarctic thermokarst ponds : investigating recent landscape evolution and sediment dynamics in thawed permafrost of Northern Québec (Canada), Arctic, Antarctic and Alpine Res., 46(1), 251-271.

Dillon, P.J., Molot, L.A.: Dissolved organic and inorganic carbon mass balances in central Ontario lakes. Biogeochemistry, 36, 29-42, 1997.

Fraysse, F., Pokrovsky, O. S., and Meunier, J.-D.: Experimental study of terrestrial plant litter interaction with aqueous solutions, Geochim. Cosmochim. Ac., 74, 70–84, 2010.

Frey, K.E., Smith, L.C.: Amplified carbon release from vast West Siberian peatlands by 2100, Geophys. Res. Letters 32, L09401, doi: 10.1029/2004GL022025, 2005.

Frey, K.E., Siegel, D.I., Smith, L.C.: Geochemistry of west Siberian streams and their potential response to permafrost degradation, Water Resources Res. 43, W03406, doi: 10.1029/2006WR004902, 2007.

Grosse, G., Jones, B., Arp, C.: Thermokarst lakes, drainage, and drained basins. In: Shroder, J. (Editor in Chief), Giardino, R., Harbor, J. (Eds.), Treatise on Geomorphology. Academic Press, San Diego, CA, vol. 8, Glacial and Periglacial Geomorphology, pp. 325-353, 2013.

Gustafsson, J.: WinHumicV for Win95/98/NT, 1999. http://amov.ce.kth.se/people/gustafjp/winhumicv.htm. A Windows version of MINTEQA2 website, Gustafsson, J.; http://www.lwr.kth.se/English /OurSoftware/vminteq/index.htm, 1999.

Jansson, M., Hickler, Th., Jonsson, A., Karlsson, J.: Links between terrestrial primary production and bacterial production and respiration in lakes in a climate gradient in subarctic Sweden. Ecosystems 11, 367-376, 2008.

Karlsson, J., Giesler, R., Persson, J., and Lundin, E.: High emission of carbon dioxide and methane during ice thaw in high latitude lakes, Geophysical Research Letters, 40(6), 1123-1127, 2013.

Karlsson, J.M., Lyon, S.W., Destouni, G. : Thermokast lake, hydrological flow and water balance indicators of permafrost change in Western Siberia, J. Hydrol., 464-465, 459-466, 2012.

Karlsson, J.M., Lyon, S.W., and Destouni, G.: Temporal behavior of lake size-distribution in a thawing permafrost landscape in Northwestern Siberia, Remote Sens., 6(1), 621-636, 2014.

Kim, K., Choi, W., Hoffmann, M. R., Yoon, H.-I., and Park, B.-K.: Photoreductive dissolution of iron oxides trapped in ice and its environmental implications, Environ. Sci. Technol., 44, 4142-4148, 2010.

Kim, K., Yoon, H.-I., and Choi, W.: Enhanced dissolution of manganese oxide in ice compared to aqueous phase under illuminated and dark conditions, Environ. Sci. Technol., 46, 13160-13166, 2012.

Kirpotin, S.N., Polishchuk, Y.M., Zakharova, E., Shirokova, L., Pokrovsky, O., Kolmakova, M., Dupré, B.: One of possible mechanisms of thermokarst lakes drainage in West-Siberian North. International Journal of Environmental Studies, 65, No 5, 631-635, 2008.

Larouche, J.R., Abbott, B.W., Bowden, W.B., Jones, J.B.: The role of watershed characteristics, permafrost thaw, and wildfire on dissolved organic carbon biodegradability and water chemistry in Arctic headwater streams, Biogeosciences Discuss., 12, 4021-4056, 2015.

Laurion, I., Vincent, W. F., MacIntyre, S., Retamal, L., Dupont, C., Francus, P., and Pienitz, R.: Variability in greenhouse gas emissions from permafrost thaw ponds, Limnol. Oceanogr., 55, 115-133, 2010.

Manasypov, R. M., Pokrovsky, O. S., Kirpotin, S. N., and Shirokova, L. S.: Thermokarst lake waters across the permafrost zones of western Siberia, The Cryosphere, 8, 1177-1193, 2014.

Milne, C.J., Kinniburgh, D.G., van Riemsdijk, W.H., Tipping, E.: Generic NICA-donnan model parameters for metal-ion binding by humic substances, Environ. Sci. Technol. 37(5), 958-971, 2003.

Muller, S., Vahatalo, A. V., Stedmon, C. A., Granskog, M. A., Norman, L., Aslam, S., Underwood, G.J.C., Dieckmann, G.S., and Thomas, D.N.: Selective incorporation of dissolved organic matter (DOM) during sea ice formation, Mar. Chem., 155, 148-157, 2013.

Novikov, S.M.: Hydrology of Bog Territories of the Permafrost Zone of Western Siberia. St Petersbourg, BBM Publ. House, 536 pp, in Russian (ISBN 978-5-9651-0339-3), 2009.

Negandhi, K., Laurion, I., Whiticar, M.J., Galand, P.E., Xu, X., and Lovejoy, C.: Small thaw ponds: An accounted source of methane in the Canadian high Arctic, Plos One, 8(11), e78204, 2013.

Pokrovsky, O. S., Shirokova, L. S., Kirpotin, S. N., Audry, S., Viers, J., and Dupré, B.: Effect of permafrost thawing on organic carbon and trace element colloidal speciation in the thermokarst lakes of western Siberia, Biogeosciences, 8, 565–583, 2011.

Pokrovsky, O.S., Shirokova, L. S., Zabelina, S. A., Vorobieva, T. Y, Moreva, O. Y., Klimov, S. I., Chupakov, A. V., Shorina, N. V., Kokryatskaya, N. M., Audry, S., Viers, J., Zouite, C., Freydier, R.: Size fractionation of trace elements in a seasonally stratified boreal lake: control of organic matter and iron colloids, Aquatic Geochemistry, 18, 115–139, 2012.

Pokrovsky, O. S., Shirokova, L. S., Kirpotin, S. N., Kulizhsky, S. P., and Vorobiev, S. N.: Impact of western Siberia heat wave 2012 on greenhouse gases and trace metal concentration in thaw lakes of discontinuous permafrost zone, Biogeosciences, 10, 5349-5365, 2013.

Pokrovsky, O.S., Shirokova, L.S., and Kirpotin, S.N.: Biogeochemistry of Thermokarst Lakes of Western Siberia, Nova Science Publ. Inc., N. Y., 163 pp., 2014.

Rautio, M., Dufresne, F., Laurion, I., Bonilla, S., Vincent, W. F., and Christoffersen, K.: Shallow freshwater ecosystems of the circumpolar Arctic, Ecoscience, 18, 204-222, 2011.

Shirokova, L. S., Pokrovsky, O. S., Kirpotin, S. N., and Dupré, B.: Heterotrophic bacterio-plankton in thawed lakes of the northern part of Western Siberia controls the CO_2 flux to the atmosphere, Int. J. Environ. Stud., 66, 433–445, 2009.

Shirokova, L. S., Pokrovsky, O. S., Viers, J., Klimov, S. I., Moreva, O. Yu., Zabelina, S. A., Vorobieva, T. Ya., and Dupré, B.: Diurnal variations of trace metals and heterotrophic bacterioplankton concentration in a small boreal lake of the White Sea basin, Ann. Limnol.-Int. J. Lim., 46, 67-75, 2010.

Shirokova, L. S., Pokrovsky, O. S., Kirpotin, S. N., Desmukh, C., Pokrovsky, B. G., Audry, S., and Viers, J.: Biogeochemistry of organic carbon, CO_2, CH_4, and trace elements in thermokarst water bodies in discontinuous permafrost zones of Western Siberia,

Biogeochemistry, 113, 573–593, 2013.

Stepanova, V.M., Pokrovsky, O.S., Viers, J., Mironycheva-Tokareva, N.P. Kosykh, N.P., Vishnyakova, E.K.: Major and trace elements in peat profiles in Western Siberia: impact of the landscape context, latitude and permafrost coverage, Applied Geochemistry, 53, 53–70, 2015.

Tank, S.E., Lesack, L.F.W., Gareis, J.A.L., Osburn, C.L., and Hesslein, R.H.: Multiple tracers demonstrate distinct sources of dissolved organic matter to lakes of the Mackenzie Delta, western Canadian Arctic, Limnol. Oceanogr., 56(4), 1297–1309, 2011.

Tank, S.E., Esslein, R.H.H., and Esack, L.F.W.L.: Northern delta lakes as summertime CO_2 absorbers within the arctic landscape, Ecosystems, 12, 144–157, 2009.

Unsworth, E.R., Warnken, K.W., Zhang, H., Davison, W., Black, F. et al.: Model predictions of metal speciation in freshwaters compared to measurements by in situ techniques, Environ. Sci. Technol. 40 (6), 1942-1949, 2006.

Vasyukova, E. V., Pokrovsky, O. S., Viers, J., Oliva, P., Dupré, B., Martin, F., and Candaudap, F.: Trace elements in organic- and iron-rich surficial fluids of the boreal zone: Assessing colloidal forms via dialysis and ultrafiltration, Geochim. Cosmochim. Ac., 74, 449–468, 2010.

Walter, K. M., Zimov, S. A., Chanton, J. P., Verbyla, D., and Chapin, F. S.III.: Methane bubbling from Siberian thaw lakes as a positive feedback to climate warming, Nature, 443, 71-75, 2006.

Walter, K. M., Chanton, J. P., Chapin III, F. S., Schuur, E.A.G., and Zimov, S.A.: Methane production and bubble emissions from arctic lakes: Isotopic implications for source pathways and ages, J. Geophys. Res, 113, G00A08, 2008.

Walter Anthony, K.M., Anthony, P., Grosse, G., and Chanton, J.: Geologic methane seeps along boundaries of Arctic permafrost thaw and melting glaciers, Nature Geoscience, 5, 419–426, 2012.

Walter Anthony, K. M. and Anthony, P.: Constraining spatial variability of methane ebullition in thermokarst lakes using point-process models, J. Geophys. Res, 118, doi:10.1002/jgrg.20087, 2013.

Walter Anthony, K. M., Zimov, S. A., Grosse, G., Jones, M. C., Anthony, P. M., Chapin III, F. S., Finlay, J. C., Mack, M. C., Davydov, S., Frenzel, P., and Frolking, S.: A shift of thermokarst lakes from carbon sources to sinks during the Holocene epoch, Nature, 511, 452-456, 2014.

Weishaar, J.L., Aiken, G.R., Bergamaschi, B.A., Fram, M.S., Fujii, R., Mopper, K.: Evaluation of specific ultraviolet absorbance as an indicator of the chemical composition and reactivity of dissolved organic carbon, Environ. Sci. Technol. 37, 4702–4708, 2003.

Yeghicheyan, D., Bossy, C., Bouhnik Le Coz, M., Douchet, C., Granier, G., Heimburger, A., Lacan, F., Lanzanova, A., Rousseau, T. C. C., Seidel, J.-L., Tharaud, M., Candaudap F., Chmeleff, J., Cloquet, C., Delpoux, S., Labatut, M., Losno, R., Pradoux, C., Sivryn Y., and Sonke, J. E.: A Compilation of silicon, rare earth element and twenty-one other trace element concentrations in the natural river water reference material SLRS-5 (NRC-CNRC), Geostand. Geoanal. Res., 37, 449-467, 2014.

Zakharova, E. A., Kouraev, A. V., Kolmakova, M. V., Mognard, N. M., Zemtsov, V. A., and Kirpotin, S. N.: The modern hydrological regime of the northern part of Western Siberia from in situ and satellite observations, Int. J. Environ. Stud., 66, 447-463, 2009.

Zakharova, E. A., Kouraev, A. V., Frédérique R., Zemtsov, V. A., Kirpotin S. N., Seasonal variability of the Western Siberia wetlands from satellite radar altimetry, J. Hydrol., 512, 366-378, 2014.

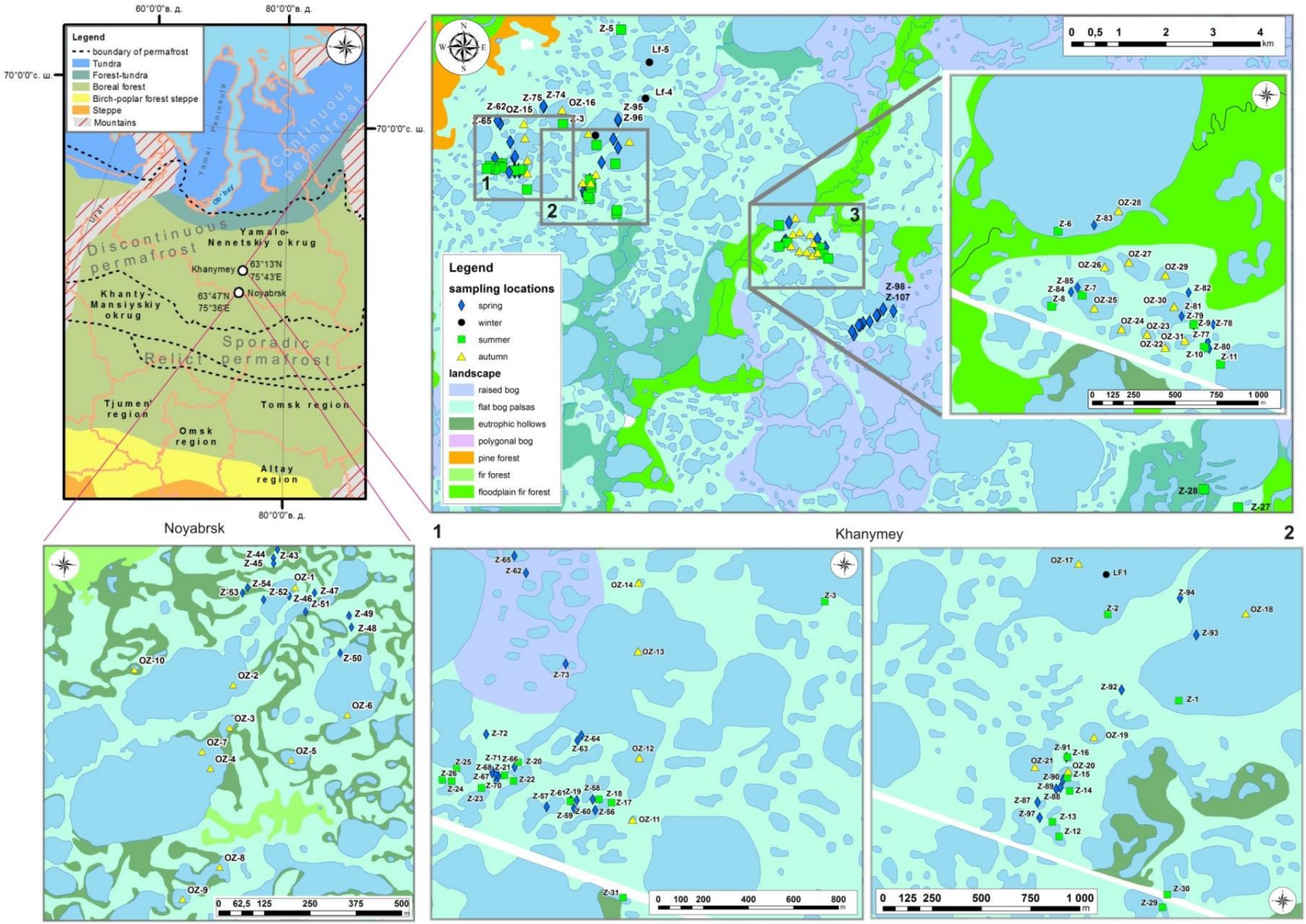

852

853 **Figure 1.** Study site area with symbols showing the position of sampled lakes and small water bodies in different seasons. Different colors correspond
854 to different elementary ecosystems.

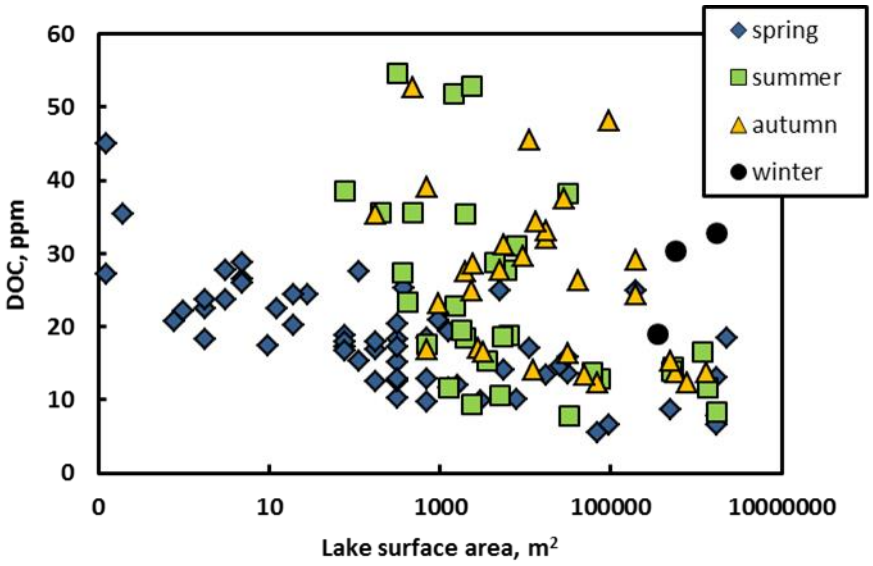

Figure 2. DOC concentration in thermokarst lakes of various size during 4 observation seasons.

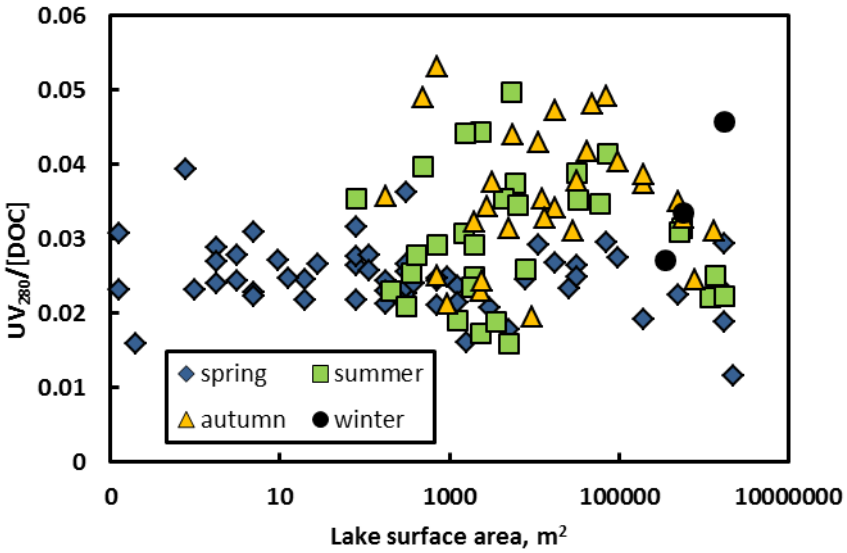

Figure 3. UV absorbence properties of thermokarst lake waters. The UV_{280}/DOC ratio increases in the order spring < summer < autumn suggesting the progressive increase of aromaticity which is independent on the lake size ($p > 0.05$). The average values of $UV_{280\ nm}$/[DOC] are equal to 0.024±0.0037, 0.030±0.0072, 0.035±0.0069, and 0.0354±0.0068 cm^{-1} in spring, summer, autumn and winter, respectively.

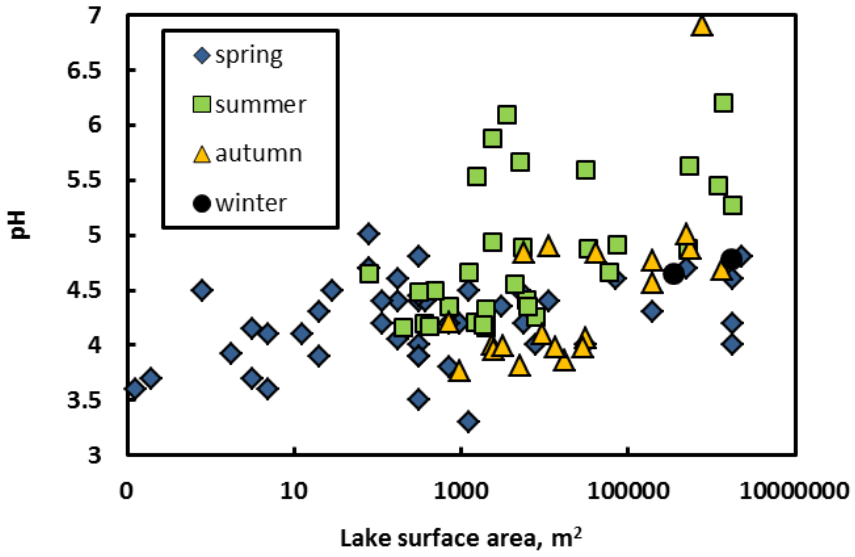

Figure 4. Increase of lake water pH with the increase of the lake size over 4 studied season. Note that the lowest pH is observed in spring and the highest in summer. This likely reflects the dominance of allochthonous organic input in the lake in spring, notably in the smallest water bodies, and autochthonous processes of some phytoplankton and macrophytes activity in the end of the summer.

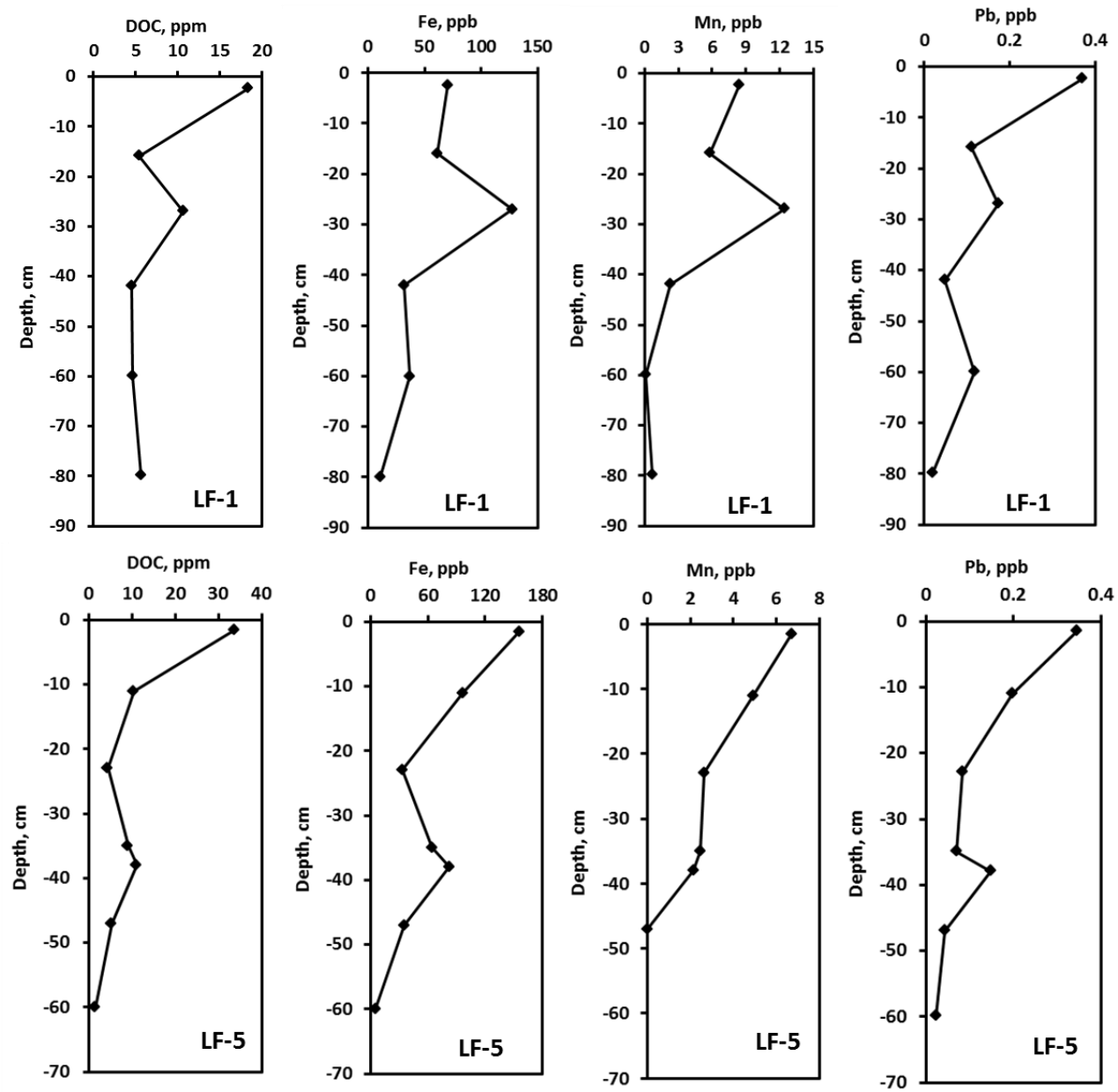

Figure 5. DOC, Fe, Mn and Pb concentration in the ice cores of thermokarst lakes sampled in February 2014

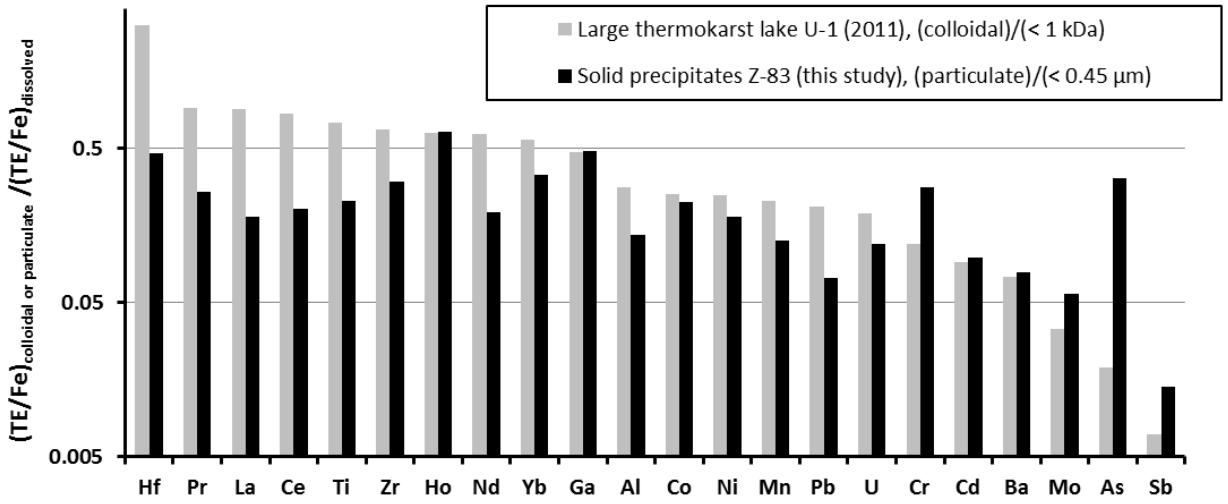

Figure 6. Comparison of the distribution coefficients of trace element (TE) normalized to Fe between the solid precipitates collected in June from the ice surface of large lake (Fig. S6) and filtered water (black columns) and those measured between colloids (1 kDa – 0.45 µm) and $LMW_{< 1\ kDa}$ fraction in large thermokarst lake (Pokrovsky et al., 2011) of discontinuous permafrost zone (grey columns).

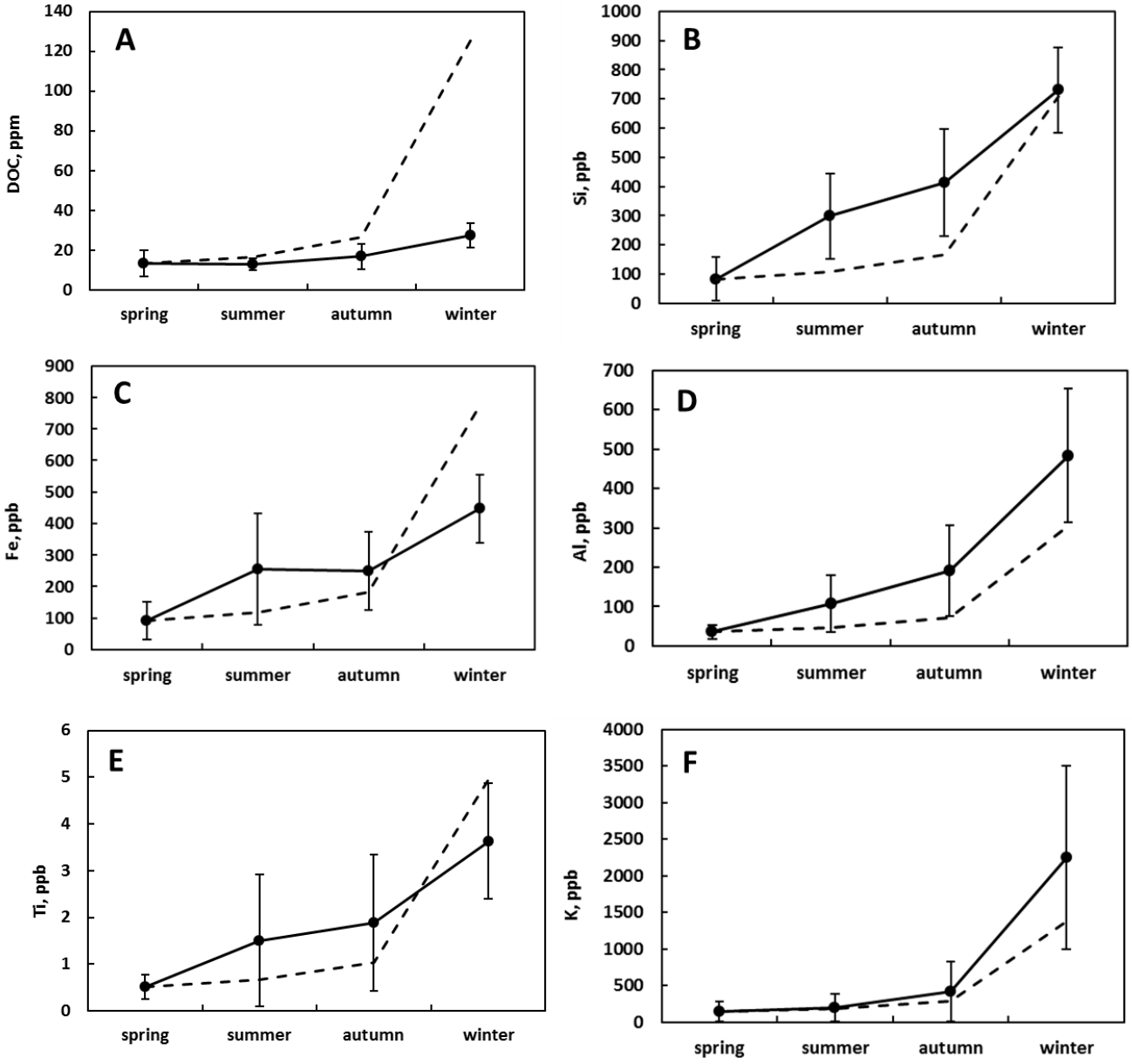

Figure 7. Size-averaged concentration of DOC (A), Si (B), Fe (C), Al (D), Ti (E), K (F), Zn (G), Cr (H), Ni (I), Cu (J), Cd (K) and Pb (L) during different seasons. The points are the average and the error bars are the standard deviation. Only the medium and large lakes (> 100 m² surface area) were used for this estimation. The dotted line represents conservative behavior for a hypothetical lake of 75 cm depth in summer, 20 cm flooding in spring, surface 20 cm ice formation in October, and almost full freezing (10 cm bottom water left) in February.

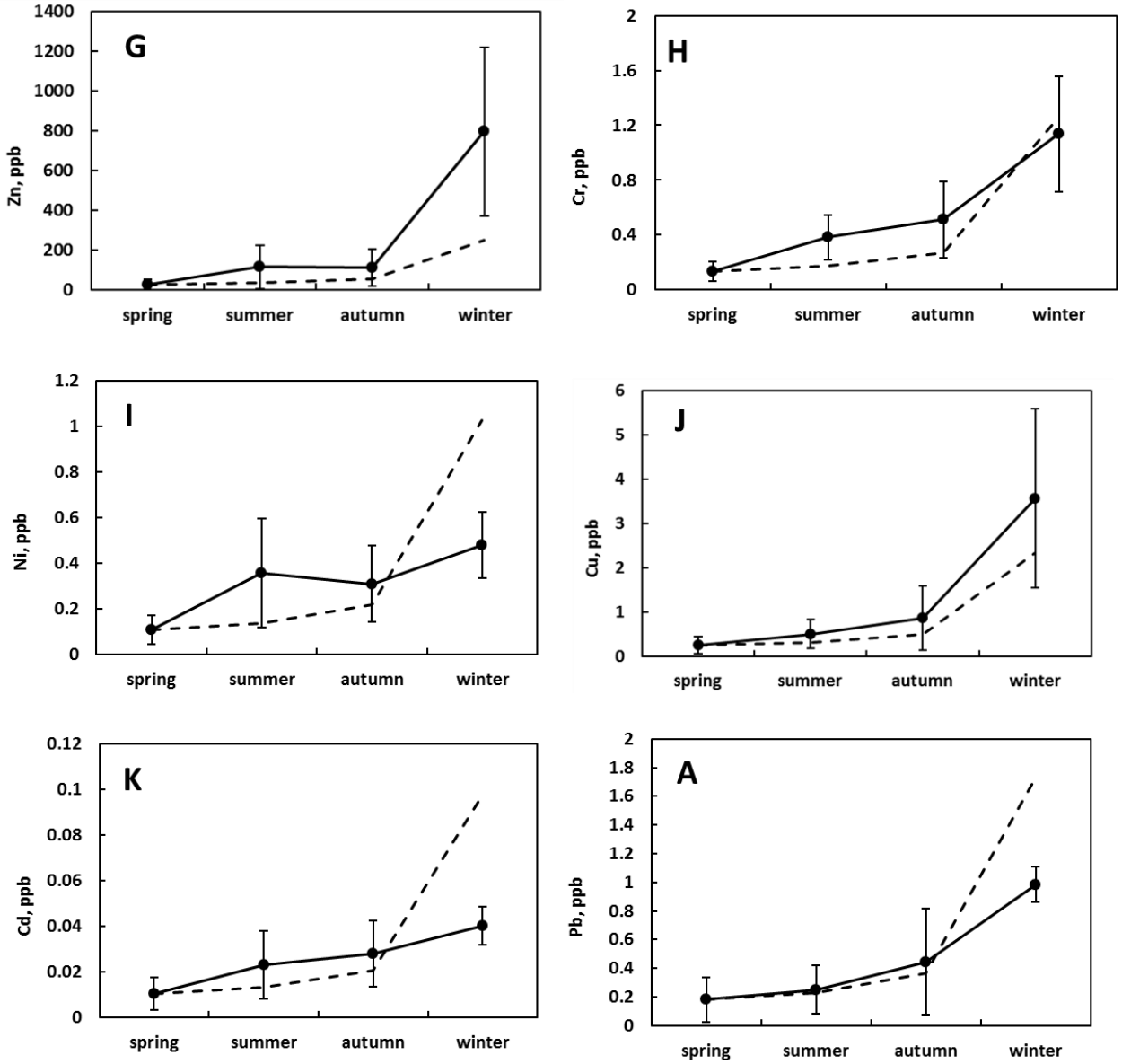

Figure 7, continued.

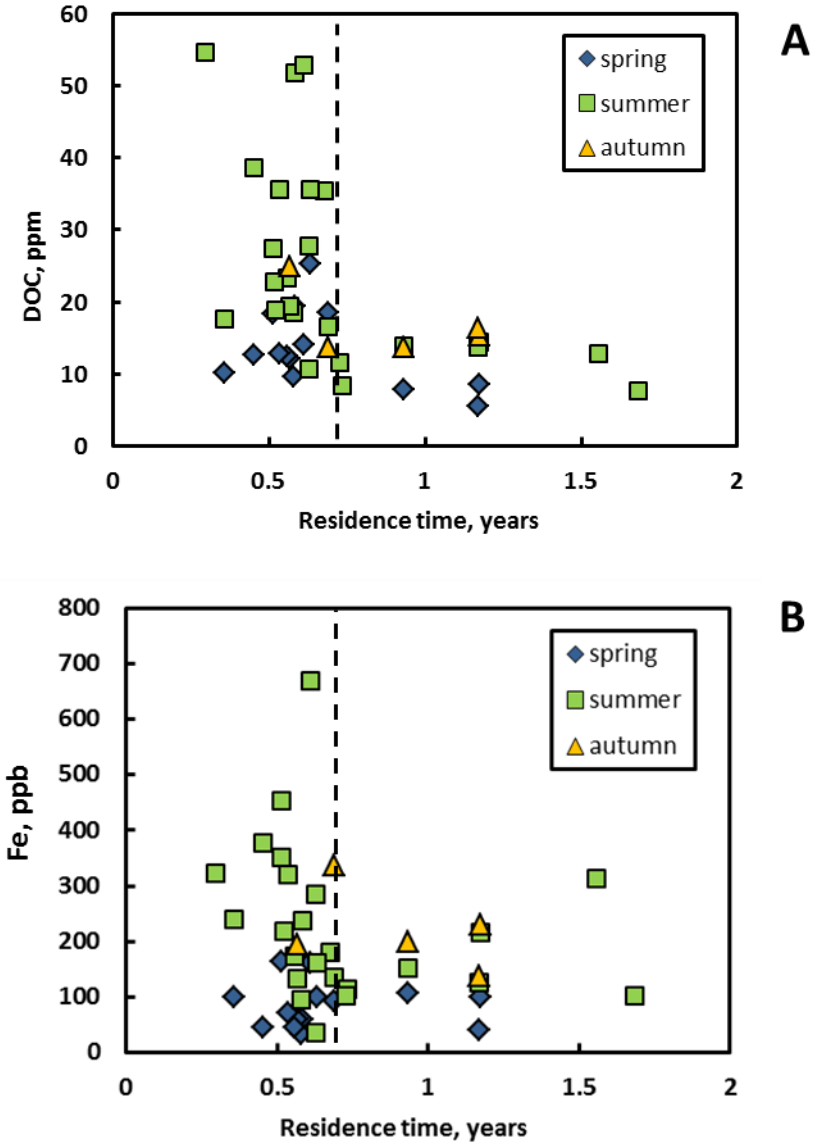

Figure 8. DOC (A) and Fe (B) concentration during different seasons plotted as a function of water residence time in the water body.

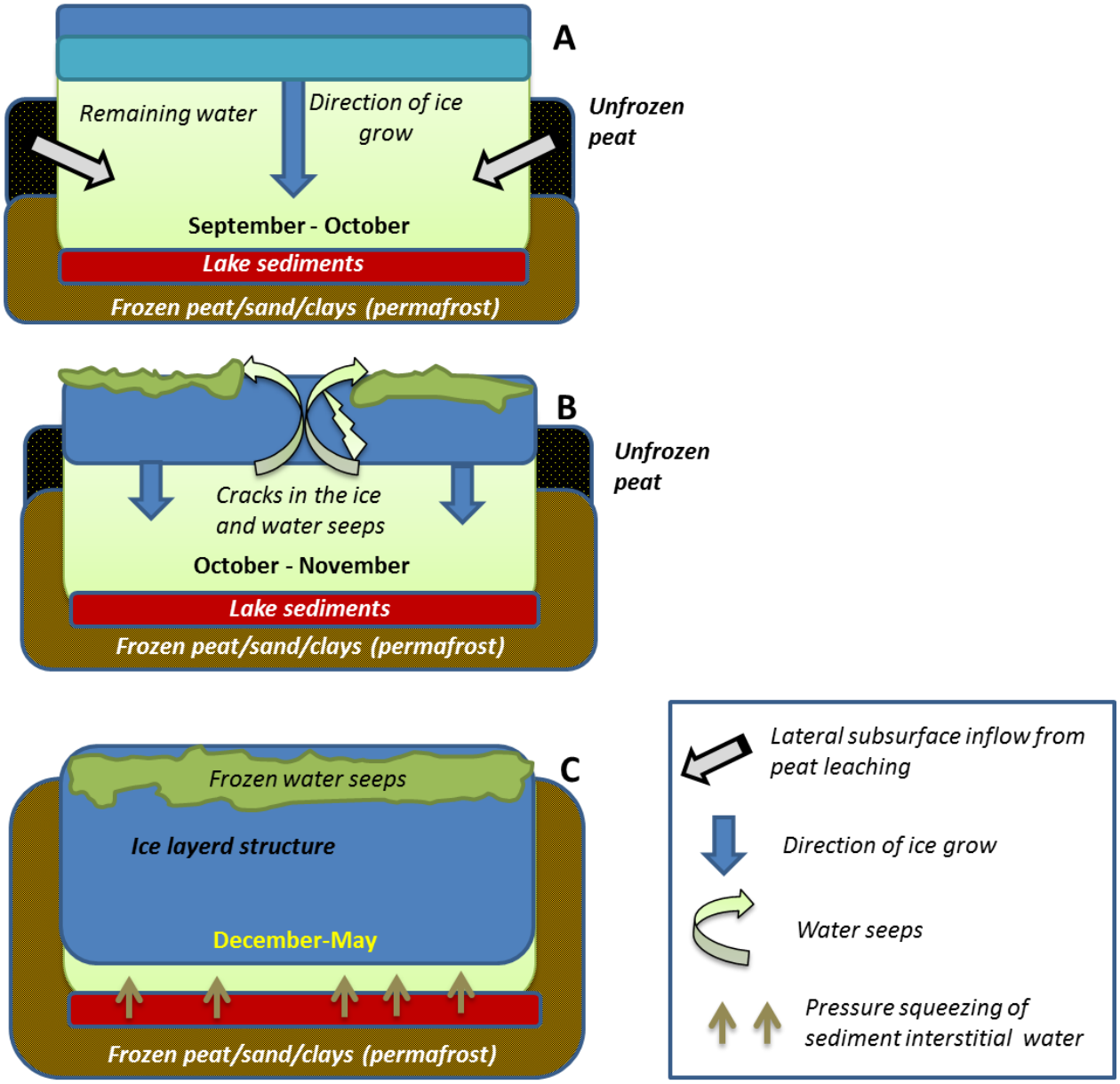

Figure 9. Sequence of ice crystallization events during the glacial period on the shallow (< 1 m depth) thermokarst lakes of western Siberia. A: start of the ice formation; B: squeezing water towards the surface via seeps; C: freezing of water pockets and seeps and multi-layer ice formation.

Table 1. Major hydrophysical and hydrochemical parameters of studied lakes.

	N	E	S, m²	T, °C	O_2, mg/L	O_2, % sat	R, µS cm^{-1}	pH	DIC, ppm	DOC, ppm	Cl, ppm	SO_4, ppm
June												
Z-43	63°13,580'	75°43,476'	**1.8**	6.5	N.D.	N.D.	N.D.	3.43	0.749	22.5	0.1532	0.9452
Z-44	63°13,567'	75°43,465'	**0.071**	7.5	N.D.	N.D.	N.D.	3.25	0.562	33.9	0.1458	0.9957
Z-45	63°13,559'	75°43,467'	**4.9**	6.0	N.D.	N.D.	N.D.	3.43	0.784	26.5	0.1466	0.8256
Z-46	63°13,513'	75°43,527'	**31400**	7.2	N.D.	N.D.	N.D.	3.28	0.396	13.6	0.0663	0.3680
Z-47	63°13,521'	75°43,608'	**1.8**	5.5	N.D.	N.D.	N.D.	3.51	0.598	23.6	0.0978	0.5896
Z-48	63°13,492'	75°43,726'	**78.5**	5.9	N.D.	N.D.	N.D.	3.49	0.433	17.2	0.0306	0.4516
Z-49	63°13,475'	75°43,737'	**1.0**	5.2	N.D.	N.D.	N.D.	3.37	0.545	22.1	0.1285	0.7087
Z-50	63°13,436'	75°43,707'	**96163**	7.5	N.D.	N.D.	N.D.	3.77	0.550	6.5	0.0848	0.4372
Z-51	63°13,492'	75°43,584'	**25434**	7.2	N.D.	N.D.	N.D.	3.08	0.435	14.7	0.0131	0.448
Z-52	63°13, 505'	75°43,444'	**17663**	6.6	N.D.	N.D.	N.D.	3.36	0.390	13.3	0.0678	0.369
Z-53	63°13,512'	75°43,374'	**9.6**	5.8	N.D.	N.D.	N.D.	3.47	0.447	17.4	0.0289	0.576
Z-54	63°13,521'	75°43,389'	**0.13**	5.5	N.D.	N.D.	N.D.	3.11	0.855	27.2	0.1337	0.752
Z-56	63°47'55,0"	75°31'21,0"	**5671.6**	3.8	9.1	86	12	4.2	0.431	14.1	0.1781	0.097
Z-57	63°47'54,4"	75°31'6,55"	**3000**	5.7	8.86	82	12	4.35	0.423	9.8	0.1637	0.616
Z-58	63°47'56,5"	75°31'19,9"	**314**	6.2	8.19	79	13	4.4	0.438	10.2	0.1616	0.595
Z-59	63°47'56,2"	75°31'14,8"	**5024**	6.0	8.3	77	30	4.5	0.437	24.9	0.0501	0.476
Z-60	63°47'55,0"	75°31'14,1"	**314.0**	6.6	8.23	78	21	4.0	0.459	15.2	0.0657	0.301
Z-61	63°47'56,1"	75°31'12,9"	**176.6**	6.5	8.2	77	17	4.05	0.410	12.5	0.0809	0.589
Z-62	63°48'28,0"	75°30'52,1"	**1766250**	5.9	8.25	79	12	4.2	0.477	13.0	0.2440	0.843
Z-63	63°48'04,7"	75°31'13,4"	**28.3**	8.5	7.33	74	20	4.5	0.394	24.5	0.024	0.233
Z-64	63°48'05,0"	75°31'14,5"	**19.6**	10.5	8.54	88	23	4.3	0.524	24.4	0.040	0.615
Z-65	63°48'29,5"	75°30'50,5"	**11304**	8.3	8.6	86	14	4.4	0.449	17.1	0.157	0.731
Z-66	63°48'00,2"	75°30'53,8"	**314.0**	9.9	8.55	85	15	4.8	0.429	12.6	0.064	0.964
Z-67	63°47'59,3"	75°30'46,8"	**78.5**	11.4	8.38	90	28	5.01	0.402	18.8	0.050	0.385
Z-68	63°47'59,0"	75°30'46,8"	**176.6**	10.2	8.46	88	22	4.4	0.378	16.9	0.043	0.725

Asterisk stands for lake sampled during all four seasons

1047 **Table 1, continued.**

	N	E	S, m²	T, °C	O_2, mg/L	O_2, % sat	R, µS cm^{-1}	pH	DIC, ppm	DOC, ppm	Cl, ppm	SO_4, ppm
Z-69	63°47'58,7"	75°30'48,8"	**314.0**	8.5	9.2	99	14	3.9	0.458	12.9	0.149	0.341
Z-70	63°47'58,0"	75°30'48,3"	**78.5**	12.5	8.25	91	18	4.7	0.378	17.9	0.040	0.505
Z-71	63°47'58,9"	75°30'47,9"	**0.0079**	N.D.	N.D.	N.D.	N.D.	N.D.	0.610	22.6	1.484	0.843
Z-72	63°48'04,5"	75°30'43,7"	**1.8**	16.5	7.5	84	30	3.92	0.390	18.2	0.170	0.860
Z-73	63°48'15,5"	75°31'07,4"	**706.5**	12.9	8.7	98	17	3.8	0.372	12.8	0.069	0.339
Z-74(A)**	63°48'39,7"	75°31'59,9"	**503289**	6.3	9.2	94	9	4.0	0.426	7.8	0.146	0.647
Z-75	63°48'39,9"	75°31'59,4"	**0.20**	17.2	8.1	82	34	3.7	0.854	35.4	0.102	0.776
Z-77	63°46'58,0"	75°39'12,2"	**113**	12.4	7.95	87	32	4.4	0.432	27.5	0.102	0.247
Z-78	63°47'01,4"	75°39'14,0"	**3.1**	10.8	7.12	77	41	3.7	0.419	27.7	0.037	0.419
Z-79	63°47'01,0"	75°39'05,4"	**314**	12.7	7.6	86	18	3.5	0.304	18.3	0.022	0.201
Z-80	63°46'56,6"	75°39'13,1"	**1256**	11.8	7.8	85	23	3.3	0.303	19.4	0.093	0.276
Z-81	63°47'01,7"	75°39'02,2"	**31400**	12	8.3	93	19	4.0	0.323	15.8	0.304	0.163
Z-82	63°47'07,2"	75°39'02,0"	**113**	14.4	8.4	97	19	4.2	0.359	15.3	0.009	0.216
Z-83(B)**	63°47'18,9"	75°38'30,1"	**1396375**	3.4	8.6	82	11	4.6	0.858	6.5	0.117	0.209
Z-84	63°47'06,7"	75°38'10,8"	**314**	15.1	7.8	90	19	3.9	0.355	17.2	0.009	0.244
Z-85(C)**	63°47'05,4"	75°38'10,4"	**53629**	10.9	7.99	80	7	4.6	0.433	5.5	0.067	0.471
Z-87	63°47'41,5"	75°33'01,0"	**1256**	13.7	8.43	95	12	4.5	0.338	11.6	0.060	0.493
Z-88	63°47'43,9"	75°33'07,5"	**177**	20.5	8.02	98	N.D.	4.6	0.325	17.9	0.031	0.260
Z-89	63°47'44,2"	75°33'09,0"	**707**	N.D.	7.4	98	N.D.	N.D.	0.285	9.7	0.189	0.215
Z-90(D)**	63°47'45,5"	75°33'09,7"	**3485**	N.D.	7.9	95	N.D.	N.D.	0.283	12.1	0.138	0.146
Z-91	63°47'49,2"	75°33'10,3"	**380**	N.D.	7.8	95	23	4.4	0.329	25.3	0.045	0.247
Z-92	63°48'01,0"	75°33'28,5"	**78.5**	20	7.7	95	12	4.7	0.334	16.6	0.014	0.255
Z-93(E)**	63°48'11,0"	75°33'54,4"	**1207054**	16	8.36	99	9	4.8	0.402	18.5	0.245	0.756
Z-94	63°48'16,8"	75°33'47,2"	**19.6**	18	8.36	104	24	3.9	0.304	20.2	0.041	0.272
Z-95	63°48'29,7"	75°33'55,0"	**4.9**	17.8	7.4	98	31	4.1	0.305	26.0	0.045	0.732
Z-96*	63°48'30,2"	75°33'54,7"	**580586**	9.3	7.9	88	8	4.7	0.550	8.6	0.166	1.011

Table 1, continued.

	N	E	S, m²	T, °C	O_2, mg/L	O_2, % sat	R, µS cm^{-1}	pH	DIC, ppm	DOC, ppm	Cl, ppm	SO4, ppm
Z-97	63°47'39,0"	75°33'02,3"	**3**	19.6	7.9	91	18	4.34	0.285	21.9	0.032	0.316
Z-98	63°46'17,2"	75°40'58,6"	**0.79**	15.6	7.27	92	19	4.5	0.282	20.7	0.108	0.317
Z-99	63°46'18,5"	75°40'42,9"	**314**	17.9	6.44	86	N.D.	4.45	0.298	20.3	0.136	0.027
Z-100	63°46'14,4"	75°40'34,2"	**3.1**	15.7	6.7	84	N.D.	4.15	0.311	23.7	0.081	0.322
Z-101	63°46'14,4"	75°40'32,5"	**7850**	13.3	6.8	80	N.D.	4.0	0.347	10.0	0.055	0.252
Z-102	63°46'10,1"	75°40'21,5"	**4.9**	12.5	5.7	70	N.D.	3.6	0.353	28.8	0.151	0.465
Z-103	63°46'09,2"	75°40'11,4"	**961.6**	19.5	6.8	88	N.D.	4.2	0.291	20.9	0.075	0.318
Z-104	63°46'07,8"	75°40'07,0"	**0.13**	17.9	5.3	71	N.D.	3.6	0.304	45.0	0.182	0.619
Z-105	63°46'07,7"	75°40'04,4"	**706.5**	14.6	6.7	80	N.D.	4.2	0.294	18.4	0.037	0.218
Z-106	63°46'01,4"	75°39'57,0"	**12.6**	18.2	6.8	90	N.D.	4.1	0.270	22.4	0.043	0.305
Z-107	63°46'03,7"	75°39'54,3"	**196250**	15.6	6.8	85	N.D.	4.31	0.293	25.0	N.D.	N.D.

Table 1, continued.

	N	E	S, m²	T, °C	O_2, mg/L	O_2, % sat	R, µS cm^{-1}	pH	DIC, ppm	DOC, ppm	Cl, ppm	SO4, ppm
August												
Z-1(E)**	63°47'57,9"	75°33'49,2"	**1207054**	N.D.	N.D.	N.D.	N.D.	5.45	0.422	16.55	0.089	0.3259
Z-2*	63°48'11,1"	75°33'23,2"	**580586**	N.D.	N.D.	N.D.	N.D.	5.63	0.440	14.40	0.187	0.6155
Z-3(A)**	63°48'27,6"	75°32'29,3"	**503289**	N.D.	N.D.	N.D.	N.D.	4.88	0.376	13.86	0.111	0.2534
Z-4	63°51'32,11"	75°37'10,6"	**33000**	N.D.	N.D.	N.D.	N.D.	4.88	0.363	7.73	0.039	0.0804
Z-5	63°49'32,1"	75°34'00,6"	**74000**	N.D.	N.D.	N.D.	N.D.	4.92	0.429	12.8	0.423	0.1880
Z-6(B)**	63°47'15,2"	75°37'58,3"	**1396375**	N.D.	N.D.	N.D.	N.D.	6.20	2.470	11.7	0.480	0.1711
Z-7(C)**	63°47'06,7"	75°38'12,2"	**53629**	N.D.	N.D.	N.D.	N.D.	4.67	0.385	13.7	0.076	0.1023
Z-8	63°47'02,3"	75°38'02,5"	**6000**	N.D.	N.D.	N.D.	N.D.	4.41	0.370	27.7	0.156	0.342
Z-9	63°47'01,1"	75°39'05,5"	**359.8**	N.D.	N.D.	N.D.	N.D.	4.20	0.403	27.4	0.098	0.200
Z-10	63°46'56,8"	75°39'10,9"	**1481.9**	N.D.	N.D.	N.D.	N.D.	4.21	0.334	51.8	0.197	0.326
Z-11	63°46'53,8"	75°39'18,6"	**1766250**	N.D.	N.D.	N.D.	N.D.	5.28	0.392	8.4	0.182	0.283
Z-12	63°47'36,2"	75°33'10,0"	**1256**	N.D.	N.D.	N.D.	N.D.	4.66	0.392	11.6	0.048	0.104
Z-13	63°47'38,5"	75°33'07,1"	**1963**	N.D.	N.D.	N.D.	N.D.	4.16	0.570	35.4	0.090	0.306
Z-14	63°47'43,8"	75°33'12,5"	**1963**	N.D.	N.D.	N.D.	N.D.	4.33	0.310	18.5	0.037	0.114
Z-15 (D)**	63°47'45,9"	75°33'11,2"	**3485**	N.D.	N.D.	N.D.	N.D.	4.19	0.301	19.5	0.038	0.072
Z-16	63°47'49,3"	75°33'10,6"	**201.0**	N.D.	N.D.	N.D.	N.D.	4.16	0.386	35.7	0.077	0.119
Z-17	63°47'56,3"	75°31'26,1"	**2374.6**	N.D.	N.D.	N.D.	N.D.	4.94	0.341	52.9	1.178	0.486
Z-18	63°47'56,6"	75°31'21,9"	**707**	N.D.	N.D.	N.D.	N.D.	4.35	0.373	17.6	0.082	0.049
Z-19	63°47'56,0"	75°31'12,7"	**415**	N.D.	N.D.	N.D.	N.D.	4.17	0.335	23.4	0.088	0.091
Z-20	63°48'00,9"	75°30'54,8"	**78.5**	N.D.	N.D.	N.D.	N.D.	4.65	0.306	38.6	0.242	0.159
Z-21	63°47'58,9"	75°30'50,8"	**491**	N.D.	N.D.	N.D.	N.D.	4.50	0.319	35.6	0.118	0.245
Z-22	63°47'58,2"	75°30'53,8"	**7850**	N.D.	N.D.	N.D.	N.D.	4.25	0.316	31.0	0.157	3.115
Z-23	63°47'56,8"	75°30'43,7"	**4416**	N.D.	N.D.	N.D.	N.D.	4.56	0.300	28.7	0.084	3.116
Z-24	63°47'57,4"	75°30'33,9"	**6359**	N.D.	N.D.	N.D.	N.D.	4.35	0.321	18.9	0.142	0.126
Z-25	63°47'59,3"	75°30'35,1"	**5408**	N.D.	N.D.	N.D.	N.D.	4.88	0.312	18.6	0.073	0.164
Z-26	63°47'57,5"	75°30'30,8"	**314**	N.D.	N.D.	N.D.	N.D.	4.48	0.340	54.7	0.193	0.280

Table 1, continued.

	N	E	S, m²	T, °C	O_2, mg/L	O_2, % sat	R, µS cm^{-1}	pH	DIC, ppm	DOC, ppm	Cl, ppm	SO_4, ppm
Z-27	63°43'59,9"	75°49'48,3"	**2375**	N.D.	N.D.	N.D.	N.D.	5.88	0.865	9.3	0.031	2.016
Z-28	63°44'12,7"	75°48'55,6"	**3524**	N.D.	N.D.	N.D.	N.D.	6.10	1.251	15.3	0.197	0.183
Z-29	63°47'26,1"	75°33'50,5"	**1520**	N.D.	N.D.	N.D.	N.D.	5.54	0.465	22.8	0.766	0.246
Z-30	63°47'28,2"	75°33'51,8"	**31400**	N.D.	N.D.	N.D.	N.D.	5.59	0.360	38.2	0.608	4.797
Z-31	63°47'42,9"	75°31'32,4"	**5024**	N.D.	N.D.	N.D.	N.D.	5.66	0.357	10.6	0.055	0.855
October												
OZ-1	63°13'31,6"	75°43'32,6"	**96163**	N.D.	N.D.	N.D.	N.D.	4.21	1.552	48.2	0.181	0.110
OZ-2	63°13'22,6"	75°43'22,1"	**17663**	N.D.	N.D.	N.D.	N.D.	4.57	0.713	32.1	0.183	0.379
OZ-3	63°13'18,8"	75°43'22,1"	**491**	N.D.	N.D.	N.D.	N.D.	5.29	1.835	52.7	0.282	0.232
OZ-4	63°13'15,1"	75°43'19,0"	**70650**	N.D.	N.D.	N.D.	N.D.	4.69	0.618	12.3	0.128	0.153
OZ-5	63°13'16,4"	75°43'34,6"	**1963**	N.D.	N.D.	N.D.	N.D.	3.75	0.536	27.5	0.115	0.128
OZ-6	63°13'20,8"	75°43'44,8"	**12266**	N.D.	N.D.	N.D.	N.D.	4.29	0.445	14.1	0.078	0.133
OZ-7	63°13'16,5"	75°43'17,1"	**49063**	N.D.	N.D.	N.D.	N.D.	4.99	0.533	13.5	0.129	0.164
OZ-8	63°13'06,5"	75°43'22,4"	**707**	N.D.	N.D.	N.D.	N.D.	4.74	1.828	39.1	0.309	0.308
OZ-9	63°13'03,4"	75°43'15,7"	**2826**	N.D.	N.D.	N.D.	N.D.	4.33	0.488	17.0	0.106	0.037
OZ-10	63°13'23,2"	75°43'02,6"	**177**	N.D.	N.D.	N.D.	N.D.	4.52	3.492	35.4	1.252	0.178
OZ-11	63°47'54,1"	75°31'33,3"	**110**	N.D.	N.D.	N.D.	N.D.	3.99	0.723	24.3	0.541	0.036
OZ-12	63°48'03,0"	75°31'33,8"	**196250**	N.D.	9.3	86	N.D.	4.57	1.264	29.2	0.201	0.746

Table 1, continued.

	N	E	S, m²	T, °C	O_2, mg/L	O_2, % sat	R, µS cm^{-1}	pH	DIC, ppm	DOC, ppm	Cl, ppm	SO_4, ppm
OZ-13	63°48'18,2"	75°31'30,4"	**196250**	N.D.	10.5/8.3	95/74	8	4.77	0.574	24.3	0.165	0.601
OZ-14	63°48'28,0"	75°31'28,7"	**707**	N.D.	12.3/10	100/94	6	4.21	0.460	16.8	0.122	0.060
OZ-15	63°48'36,8"	75°31'38,1"	**41527**	N.D.	8.8/7.2	74/64	N.D.	4.84	0.650	26.3	0.224	0.248
OZ-16(A)**	63°48'37,3"	75°32'28,2"	**503289**	N.D.	7.4/6.2	67/56	N.D.	4.87	0.581	13.7	0.194	0.314
OZ-17*	63°48'21,0"	75°33'08,6"	**580586**	N.D.	9.1/6.9	80/66	N.D.	5.01	0.507	15.3	0.284	0.316
OZ-18(E)**	63°48'15,2"	75°34'12,0"	**1207054**	N.D.	8.1/7.3	80/68	N.D.	4.69	0.495	13.7	0.193	0.708
OZ-19	63°47'52,9"	75°33'19,8"	**9499**	N.D.	8.6/5.8	78/55.2	N.D.	4.10	0.602	29.6	0.074	0.247
OZ-20(D)**	63°47'47,0"	75°33'11,3"	**3485**	N.D.	11.7/10.3	101/97	N.D.	4.01	0.596	24.9	0.179	0.052
OZ-21	63°47'47,2"	75°32'58,9"	**11304**	N.D.	10.1/4.7	92/44	N.D.	4.91	0.530	45.6	0.464	1.410
OZ-22	63°46'56,1"	75°38'53,7"	**2462**	N.D.	8.25/5.87	72/53	N.D.	3.96	0.508	28.6	0.246	1.566
OZ-23	63°46'58,4"	75°38'45,2"	**5024**	N.D.	4.2/3.34	38/30	N.D.	3.81	0.662	27.7	0.828	0.878
OZ-24	63°46'59,0"	75°38'33,8"	**3215**	N.D.	5.1/4.5	46/40	N.D.	3.99	0.595	16.5	0.140	0.121
OZ-25 (C)**	63°47'02,6"	75°38'21,2"	**53629**	N.D.	9.2/4.4	85/41	N.D.	4.06	0.556	16.3	0.095	0.204
OZ-26	63°47'10,8"	75°38'24,2"	**5672**	N.D.	8.3/4.0	75/38	N.D.	4.85	0.820	31.1	0.234	2.909
OZ-27	63°47'12,1"	75°38'34,64"	**17663**	N.D.	7.8/5.4	79/49	N.D.	3.87	0.466	33.1	0.164	0.535
OZ-28 (B)**	63°47'21,9"	75°38'28,2"	**1396375**	N.D.	9.75	87	N.D.	6.90	2.920	12.3	0.543	1.686
OZ-29	67°47'10,2"	75°38'51,1"	**28339**	N.D.	4.2/5.4	37/49	N.D.	3.98	0.488	37.5	0.170	0.606
OZ-30	63°47'04,2"	75°38'56,1"	**13267**	N.D.	4.2/5.8	37/51	N.D.	3.98	0.444	34.4	0.187	0.669
OZ-31	63°46'57,8"	75°39'02,1"	**962**	N.D.	4.5/3.9	40/35	N.D.	3.77	0.469	23.1	0.229	0.186
February												
LF1* bottom	63˚48'19.6"	75˚33'19.2"	**580586**	N.D.	N.D.	N.D.	N.D.	N.D.	0.496	30.3	0.792	3.440
LF4 bottom	63˚48'44.7"	75˚34'37.3"	**351335**	N.D.	N.D.	N.D.	19	4.655	0.778	19.0	0.235	1.678
LF5 bottom	63˚49'09.4"	75˚34'44.1"	**1743000**	N.D.	N.D.	N.D.	31	4.778	1.022	32.9	0.281	2.973

Footnote: Oxygen concentration in samples OZ-13 to OZ-31 represents surface/bottom values. Highlighted lakes (A, B, C, D, and E), **, were sampled during all open water seasons. *R* stands for specific conductivity and N.D. for non determined. * stands for a lake sampled during all four seasons.

Table 2. Distribution coefficient of soluble components between the lake water and the ice (average of 3 samples with 2 s.d.). The lower part of the ice column, formed in quasi-equilibrium with the remaining bottom water, was used for this estimation.

Element	K_d (water)/(ice)
DIC	1.64±0.37
DOC	10.3±7.0
Cl-	7.58±3.0
SO4	44.1±10.9
Na	21.2±3.4
Mg	17.9±5.4
Al	93.1±32.9
Si	12.4±5.2
K	45.8±24.1
Ca	10.2±5.2
Ti	50±20
V	22.9±3.5
Cr	20.7±8.9
Mn	117±35
Fe	67.8±12.4
Ni	16.6±2.7
Cu	46.8±21.5
Ga	34.9±12.1
As	46.4±9.8
Rb	41.7±14.4
Sr	20.2±12.7
Cd	7.4±1.7
Sb	10.9±1.9
Cs	5.7±2.1
Ba	27.2±9.3
La	41.3±16.2
Ce	58.8±21.0
Pr	45.8±38.5
Nd	52.4±9.6
Sm	26.7±13.9
Eu	49.0±32.5
Gd	21.6±1.6
Dy	47.5±34.5
Ho	14.4±11.2
Er	23.4±7.9
Yb	19.1±12.4
Pb	41.5±12.2
U	11.5±2.9

Table 3. Average concentrations and standard deviation (±2σ)of major and trace elements during different seasons of the year for two size classes of thermokarst lakes, 100-500000 m^2 and >500000 m^2. Considering all elements simultaneously, the difference between two size classes is statistically significant (p = 0.007, 0.0008 and 0.00007 for spring, summer and autumn) as follows from Wilcoxon t-test.

Element	units	100–500000 m^2				>500000 m^2			
		spring	summer	autumn	winter	spring	summer	autumn	winter
DOC	mg/L	15.2±5.1	25.6±13.3	28±10.9	n.d.	13.2±6.6	12.9±2.8	16.8±6.2	27.4±6.03
DIC	mg/L	0.38±0.07	0.42±0.2	0.79±0.67	n.d.	0.5±0.18	0.49±0.17	1.15±0.93	0.77±0.21
Cl^-	mg/L	0.09±0.06	0.13±0.11	0.21±0.16	n.d.	0.18±0.05	0.21±0.14	0.28±0.13	0.44±0.25
SO_4^{2-}	mg/L	0.37±0.2	0.44±0.41	0.43±0.38	n.d.	0.69±0.27	0.33±0.15	0.75±0.5	2.33±0.65
Specific cond.	µS cm^{-1}	17.9±5.98	n.d.	7±1	n.d.	9.8±1.47	n.d.	n.d.	25±6
pH		4.2±0.34	4.72±0.58	4.17±0.38	n.d.	4.44±0.29	5.49±0.44	5.21±0.86	4.72±0.06
Be	µg/L	0.004±0.001	0.007±0.004	0.013±0.008	n.d.	0.002±0.001	0.012±0.003	0.013±0.005	
B	µg/L	42.4±41.8	28.7±26.5	76.6±66.3	n.d.	8.22±7.61	30.1±20.3	223±169	776±413
Na	µg/L	866±854	1220±1197	910±608	n.d.	997±782	896±351	1396±925	6519±3818
Mg	µg/L	99.5±35	229±186	150±76.6	n.d.	62.2±38.4	125±12.7	199±48.3	316±137
Al	µg/L	34.7±18.3	101±69.4	181±114	n.d.	41.7±15.4	137±77.7	238±110	484±169
K	µg/L	124±123	207±203	302±227	n.d.	256±144	272±95.6	447±253	2251±1254
Ca	µg/L	211.4±92.7	289±160	309±152	n.d.	213±167	470±367	661±438	893±406
Ti	µg/L	0.512±0.27	1.16±0.664	1.76±1.3	n.d.	0.569±0.229	4.46±2.75	4.44±4.01	3.63±1.24
V	µg/L	0.272±0.088	0.363±0.252	0.484±0.361	n.d.	0.415±0.205	0.848±0.374	0.882±0.402	1.33±0.298
Cr	µg/L	0.138±0.075	0.366±0.166	0.477±0.274	n.d.	0.157±0.045	0.457±0.125	0.651±0.238	1.14±0.423
Mn	µg/L	6.25±4.39	15.7±9.92	14.6±8.95	n.d.	4.14±3.52	17.9±4.02	21.1±8.77	26.3±11.7
Fe	µg/L	84.4±57.3	251±162	230±111	n.d.	127±63	273±240	336±146	447±108
Co	µg/L	0.037±0.018	0.103±0.05	0.141±0.064	n.d.	0.029±0.016	0.095±0.035	0.093±0.039	0.215±0.034
Ni	µg/L	0.108±0.067	0.316±0.149	0.299±0.171	n.d.	0.106±0.04	0.557±0.425	0.351±0.141	0.477±0.145
Cu	µg/L	0.252±0.207	0.47±0.289	0.789±0.691	n.d.	0.208±0.07	0.634±0.439	1.2±0.768	3.56±2.01
Zn	µg/L	27.1±23.3	62.2±47	114±97.8	n.d.	27.8±26.2	108±97.3	314±276	794±423
Ga	µg/L	0.01±0.004	0.023±0.016	0.042±0.033	n.d.	0.007±0.004	0.037±0.023	0.06±0.031	0.146±0.069
As	µg/L	0.371±0.093	0.636±0.191	0.612±0.288	n.d.	0.371±0.069	0.626±0.057	0.658±0.182	0.944±0.3
Rb	µg/L	0.147±0.141	0.213±0.205	0.328±0.294	n.d.	0.275±0.069	0.388±0.166	0.92±0.536	2.07±0.963
Sr	µg/L	2.84±1.42	5.91±3.96	8±5.53	n.d.	3.12±1.6	8.94±4.72	13±6.22	29.5±12.6
Zr	µg/L	0.243±0.2	0.1±0.068	0.216±0.165	n.d.	0.488±0.011	0.309±0.138	0.612±0.359	2.06±1.8

Nb	µg/L	0.015±0.011	0.014±0.012	0.024±0.023	n.d.	0.013±0.002	0.024±0.012	0.02±0.015	0.024
Mo	µg/L	0.012±0.007	0.01±0.009	0.021±0.015	n.d.	0.023±0.008	0.021±0.003	0.021±0.009	0.033±0.017
Cd	µg/L	0.01±0.007	0.024±0.015	0.028±0.013	n.d.	0.0005	0.017±0.01	0.025±0.019	0.04±0.008
Sb	µg/L	0.04±0.014	0.046±0.012	0.077±0.031	n.d.	0.037±0.01	0.064±0.015	0.08±0.027	0.14±0.044
Cs	µg/L	0.008±0.007	0.008±0.007	0.007±0.006	n.d.	0.003±0.002	0.013±0.007	0.023±0.013	0.027±0.011
Ba	µg/L	49.5±48.9	126.4±81.2	410±393	n.d.	63.5±61.8	139±77.3	466±367	1107±446
La	µg/L	0.01±0.007	0.037±0.031	0.052±0.041	n.d.	0.003±0.002	0.072±0.02	0.071±0.016	0.221±0.016
Ce	µg/L	0.021±0.014	0.09±0.083	0.122±0.114	n.d.	0.001±0.0009	0.15±0.052	0.14±0.02	0.561±0.04
Pr	µg/L	0.004±0.003	0.011±0.01	0.016±0.015	n.d.	n.d.	0.018±0.006	0.017±0.003	0.065±0.007
Nd	µg/L	0.016±0.011	0.047±0.045	0.059±0.055	n.d.	0.028±0.007	0.078±0.026	0.074±0.011	0.215±0.022
Sm	µg/L	0.007±0.005	0.012±0.011	0.018±0.017	n.d.	0.011±0.005	0.019±0.007	0.018±0.006	0.063±0.005
Eu	µg/L	0.013±0.012	0.019±0.018	0.036±0.034	n.d.	0.022±0.018	0.014±0.005	0.035±0.032	0.142±0.052
Gd	µg/L	0.009±0.006	0.013±0.011	0.019±0.017	n.d.	0.015±0.003	0.019±0.007	0.021±0.005	0.068±0.008
Dy	µg/L	0.011±0.009	0.012±0.009	0.016±0.015	n.d.	0.023±0.004	0.019±0.005	0.02±0.005	0.061±0.012
Ho	µg/L	0.002±0.001	0.003±0.002	0.005±0.004	n.d.	n.d.	0.004±0.002	0.004±0.0008	0.018±0.004
Er	µg/L	0.015±0.013	0.006±0.005	0.01±0.009	n.d.	0.029±0.002	0.012±0.003	0.013±0.002	0.041±0.008
Tm	µg/L	0.002±0.001	0.002±0.001	0.002±0.001	n.d.	n.d.	0.002±0.001	0.002±0.0009	0.009±0.001
Yb	µg/L	0.011±0.009	0.006±0.005	0.007±0.005	n.d.	0.021±0.003	0.01±0.003	0.013±0.004	0.04±0.007
Lu	µg/L	0.002±0.001	0.002±0.001	0.002±0.001	n.d.	n.d.	0.002±0.001	0.002±0.0006	0.01±0.005
Hf	µg/L	0.0065±0.0015	0.007±0.006	0.01±0.008	n.d.	0.0034±0.0015	0.012±0.003	0.012±0.007	0.034±0.026
W	µg/L	0.016±0.009	0.083±0.081	0.115±0.112	n.d.	0.018±0.004	0.059±0.046	0.068±0.054	0.026±0.019
Pb	µg/L	0.199±0.165	0.266±0.181	0.487±0.394	n.d.	0.094±0.057	0.184±0.067	0.256±0.094	0.985±0.124
Th	µg/L	0.015±0.048	0.011±0.009	0.015±0.01	n.d.	0.011±0.007	0.023±0.007	0.018±0.009	0.026±0.006
U	µg/L	0.003±0.002	0.006±0.005	0.009±0.008	n.d.	n.d.	0.01±0.005	0.008±0.004	0.029±0.01

1089